Estimation of RVoG Scene Parameters by Means of PolInSAR With TanDEM-X Data: Effect of the Double-Bounce Contribution

Noelia Romero-Puig, *Student Member, IEEE*, Juan M. Lopez-Sanchez, *Senior Member, IEEE*, and J. David Ballester-Berman

***Abstract*— This article evaluates the effect of the double-bounce (DB) decorrelation term that appears in single-pass bistatic acquisitions, as in the TanDEM-X system, on the inversion of scene parameters by means of polarimetric SAR interferometry (PolInSAR). The retrieval of all scene parameters involved in the Random Volume over Ground (RVoG) model (i.e., ground topography, vegetation height, extinction, and ground-to-volume ratios) is affected by this term when the radar response from the ground is dominated by the DB. The estimation error in all these parameters is analyzed by means of simulations over a wide range of system configurations and scene variables for both agricultural crops and forest scenarios. Simulations demonstrate that the inclusion of the DB term, which complicates the inversion algorithm, is necessary for the angles of incidence shallower than 30° to achieve an estimation error below 10% in vegetation height and to avoid a significant underestimation in the ground-to-volume ratios. At steep incidences, this decorrelation term does not affect the estimation of vegetation height and ground-to-volume ratios. Regarding the extinction, this parameter is intrinsically not well estimated, since most retrieved values are close to the initial guesses employed for the optimization algorithm, regardless of the use or not of the DB decorrelation term. Finally, these findings are compared with the experimental results from the TanDEM-X data acquired over the rice fields in Spain for the available system parameters (baseline and incidence angle) of the acquired data set.**

***Index Terms*— Agriculture, bistatic radar, double bounce (DB), forest, polarimetric SAR interferometry (PolInSAR), rice, TanDEM-X, vegetation.**

I. Introduction

POLARIMETRIC SAR interferometry (PolInSAR) [1] has the potential for providing valuable structural metrics of vegetation covers. Evidence of this potential was found in successful results for the estimation of forest height and other key parameters with data acquired by airborne sensors [2]–[5] and, more recently, also with the TanDEM-X data [6]–[9]. Regarding agricultural crops, PolInSAR has been successfully exploited also with data from airborne campaigns [10]–[13] and from TanDEM-X [14]–[17]. In all cases, a simplified physical model of the scene, called Random Volume over Ground (RVoG), was employed to relate the PolInSAR observations to the physical properties of the scene and, consequently, to carry out the retrieval of the scene parameters defined in the model: ground topography, vegetation height, extinction, and ground-to-volume power ratios [2], [18]–[20].

Spaceborne PolInSAR data exploited in vegetation applications prior to TanDEM-X were acquired in a repeat-pass configuration: a radar operating in the monostatic mode collects sets of multipolarized SAR images over the same area at different acquisition dates. In contrast, TanDEM-X is characterized by a single-pass acquisition mode resulting from its bistatic configuration, i.e., only one satellite acts as a transmitter and both of them act simultaneously as receivers. These two acquisition modes differ in two aspects concerning the formulation of the interferometric coherence in the RVoG model. In the first place, the vertical wavenumber is scaled by a factor of 2 in the repeat-pass systems with respect to the single-pass or bistatic systems, since the one-way path from the satellite to the scene is common to the two images in the single-pass systems, whereas it is different in the repeat-pass systems [19]. The second difference is that, in bistatic acquisitions, when a double-bounce (DB) contribution is present at the ground (as a result of the interaction between the trunks or stems and the ground), the interferometric coherence is affected by an extra decorrelation factor [18]. Treuhaft *et al.* [18] and Treuhaft and Siqueira [19] originally defined this term, and later on, Ballester-Berman and Lopez-Sanchez [21], [22] analyzed it from a theoretical point of view. Unfortunately, until the operation of TanDEM-X, this formulation could not be tested on real data. However, all the experiments illustrated in the literature using PolInSAR with TanDEM-X data for forests [6]–[9] and most of the crop cases [14], [16], [17] have ignored the mentioned decorrelation term, and the vegetation heights obtained were accurate enough. Therefore, to date, the real extent of the influence of this term on the retrieval of the scene parameters still remains unclear.

The aim of this article is to provide, for the first time, a detailed analysis of the effect of the DB decorrelation term on the inversion of the RVoG scene parameters. The analysis

Manuscript received July 18, 2019; revised December 10, 2019 and January 20, 2020; accepted March 12, 2020. This work was supported in part by the Spanish Ministry of Science, Innovation and Universities, the State Agency of Research (AEI), and in part by the European Funds for Regional Development (EFRD) under Project TEC2017-85244-C2-1-P. The work of Noelia Romero-Puig was supported in part by the Generalitat Valenciana and in part by the European Social Fund (ESF) under Grant ACIF/2018/204. *(Corresponding author: Noelia Romero-Puig.)*

The authors are with the Institute for Computer Research (IUII), University of Alicante, E-03080 Alicante, Spain (e-mail: noelia.romero@ua.es; juanma-lopez@ieee.org; davidb@ua.es).

Color versions of one or more of the figures in this article are available online at http://ieeexplore.ieee.org.

Digital Object Identifier 10.1109/TGRS.2020.2981756

is not limited to vegetation height but to the whole set of scene parameters, i.e., including extinction and ground-to-volume ratios. Taking as a starting point the retrieval algorithm presented in [15] and completing the initial analysis shown in [23], this article is aimed to answer the following questions.

1) Is it necessary to consider the DB decorrelation term in the estimation of scene parameters? What is the error when it is ignored?
2) Are the estimates of all model parameters affected equally? or some parameters are affected more by others?
3) Under which scene properties (model parameter values) and system configurations (baseline and incidence angle) the impact on the retrieval is negligible?

This article is organized as follows. Section II outlines the theoretical PolInSAR background and the RVoG model. In Section III, the inversion strategy for the estimation of the scene parameters is described. Section IV evaluates the inversion strategy with the simulated data for which the results are presented and discussed. Section V presents the results with real data. Finally, the conclusions are drawn in Section VI.

II. Theoretical Background

A. Polarimetric SAR Interferometry

Polarimetric SAR systems combine sets of images acquired at multiple polarimetric channels. In TanDEM-X dual-pol interferometry, selecting HH and VV as the two polarimetric channels [6], each dual-pol image is expressed as a 2-D scattering vector, $\vec{k}_1$ and $\vec{k}_2$, in the Pauli basis [1]

$$\vec{k}_j = \frac{1}{\sqrt{2}}\left[S^j_{\mathrm{HH}} + S^j_{\mathrm{VV}}, \quad S^j_{\mathrm{HH}} - S^j_{\mathrm{VV}}\right]^T \quad \forall j = 1, 2 \tag{1}$$

where S^j_{PP} represents the complex scattering amplitude at the jth end of the spatial baseline with PP polarization (PP = HH, VV). A scattering amplitude $S(\vec{w})$ is formed by a projection of the scattering vector $\vec{k}$ on a unitary complex vector $\vec{w}$ that specifies the selected polarimetric combination [1], [24], yielding

$$S_1(\vec{w}) = \vec{w}^{*^T}\vec{k}_1, \quad S_2(\vec{w}) = \vec{w}^{*^T}\vec{k}_2 \tag{2}$$

assuming the same polarization for both images $\vec{w}_1 = \vec{w}_2 = \vec{w}$.

The generalized vector expression for the complex interferometric coherence γ is then the following:

$$\gamma(\kappa_Z, \vec{w}) = \frac{\vec{w}^{*T}[\Omega_{12}(\kappa_Z)]\vec{w}}{\sqrt{(\vec{w}^{*T}[T_{11}]\vec{w})(\vec{w}^{*T}[T_{22}]\vec{w})}} \tag{3}$$

where

$$\begin{aligned}[\Omega_{12}(\kappa_Z)] &= \langle \vec{k}_1 \cdot \vec{k}_2^{*T} \rangle \\ [T_{11}] &= \langle \vec{k}_1 \cdot \vec{k}_1^{*T} \rangle \\ [T_{22}] &= \langle \vec{k}_2 \cdot \vec{k}_2^{*T} \rangle.\end{aligned} \tag{4}$$

In (4), matrices $[T_{11}]$ and $[T_{22}]$ contain the polarimetric information, $[\Omega_{12}(\kappa_Z)]$ contains the polarimetric information and the interferometric information, and the operator $\langle\cdot\rangle$ indicates spatial multilooking. The vertical interferometric wavenumber κ_Z, as specified in [18] and [19] for bistatic systems

$$\kappa_Z = \frac{2\pi B_\perp}{\lambda R \sin\theta_0} \tag{5}$$

depends on the perpendicular baseline $B_\perp$, the wavelength λ, and the incidence angle θ_0.

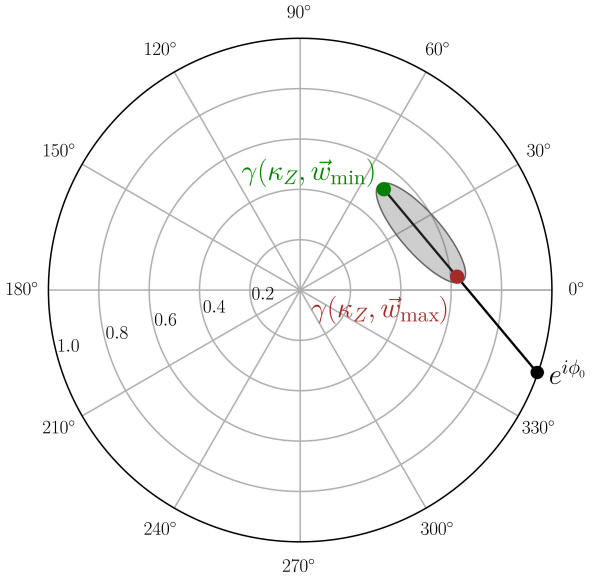

Fig. 1. Unit circle on the complex plane representing the coherence region (gray ellipse), the coherences with minimum ground contribution $\gamma(\kappa_Z, \vec{w}_{\min})$ (green dot), and maximum ground contribution $\gamma(\kappa_Z, \vec{w}_{\max})$ (red dot), and the line of the standard RVoG model crossing the unit circumference at the topographic phase ϕ_0.

The coherence region (gray ellipse in Fig. 1) provides the geometrical interpretation of the interferometric coherences $\gamma(\kappa_Z, \vec{w}_j)$ on the complex plane within the unit circle [25], [26]. By varying the projection vector $\vec{w}$, the coherence region represents the polarimetric interferometric signature of the observed scene, thus providing a way of quantifying the sensitivity of the PolInSAR data to the scene properties.

B. RVoG Model

The retrieval of the vegetation parameters by means of PolInSAR is based on the inversion of a simplified electromagnetic model of the scene. The most widely used model is the RVoG [2], [18]–[20], which describes the scene as a two-layer medium comprised of a homogeneous volume of randomly oriented scatterers (e.g., stalks and leaves for crops; leaves, branches, and trunks for forests), distributed along the vertical coordinate according to a scattering function $f(z)$ on the top of an impenetrable ground surface, located at $z = z_0$.

Regarding this assumption, the most complete expression of the PolInSAR coherence $\tilde{\gamma}(\kappa_Z, \vec{w})$ at different polarimetric channels $\vec{w}$ for a bistatic system, accounting for the two contributions of the ground (surface or direct scattering, and DB scattering) [6], [18], [19], [21], is as follows:

$$\tilde{\gamma}(\kappa_Z, \vec{w}) = e^{i\phi_0}\frac{\tilde{\gamma}_V + \mu_{\mathrm{D}}(\vec{w}) + \gamma_{\mathrm{DB}}\mu_{\mathrm{DB}}(\vec{w})}{1 + \mu_{\mathrm{D}}(\vec{w}) + \mu_{\mathrm{DB}}(\vec{w})} \tag{6}$$

where $\phi_0 = \kappa_Z z_0$ is the topographic phase (i.e., the interferometric phase at the ground level), and $\mu_{\mathrm{D}}(\vec{w})$ and $\mu_{\mathrm{DB}}(\vec{w})$ are the ground-to-volume backscatter ratios corresponding to the direct (D) and DB contributions, respectively. The term $\tilde{\gamma}_V$ is the coherence of the volume layer, characterized by a height h_v, without any ground contribution. It is expressed as a function of $f(z)$ as

$$\tilde{\gamma}_V = \frac{\int_0^{h_v} f(z) e^{i\kappa_Z z} dz}{\int_0^{h_v} f(z) dz}. \tag{7}$$

The first factor in the third term of the numerator in (6), γ_{DB}, is the DB decorrelation term that appears whenever a bistatic configuration is used

$$\gamma_{\mathrm{DB}} = \frac{\sin k_z h_v}{k_z h_v}. \tag{8}$$

Note that the wavenumber in (8) is k_z, not κ_Z, and it is defined as follows (see [18], [19], [21], [22] for more details):

$$k_z = \kappa_Z \sin^2 \theta_0. \tag{9}$$

In many natural scenes, the direct response from the ground is the dominant ground contribution, and thus, the coherence expression would be simplified as

$$\tilde{\gamma}(\kappa_Z, \vec{w}) = e^{i\phi_0} \frac{\tilde{\gamma}_V + \mu_{\mathrm{D}}(\vec{w})}{1 + \mu_{\mathrm{D}}(\vec{w})}. \tag{10}$$

In other scenarios, e.g., rice fields [14], [15] and mangroves [8], [17], the ground is flooded, which favors the DB contribution and makes negligible the direct contribution. In such a case, the dominant ground contribution is the DB, and the coherence expression turns into

$$\tilde{\gamma}(\kappa_Z, \vec{w}) = e^{i\phi_0} \frac{\tilde{\gamma}_V + \gamma_{\mathrm{DB}} \mu_{\mathrm{DB}}(\vec{w})}{1 + \mu_{\mathrm{DB}}(\vec{w})}. \tag{11}$$

Whenever there is no clear dominance of one of the two ground contributions, i.e., the direct D or the DB, the most general expression of coherence (6) should be used [22].

Different approaches have been proposed to model the vegetation volume structure and, hence, the scattering function $f(z)$, being the most common an exponential function governed by an extinction coefficient σ. In many agricultural crops, the scatterers within the volume may share a predominant vertical orientation, leading to a larger attenuation of the waves in the vertical polarization. The model that accounts for this dependence is the Oriented Volume over Ground (OVoG) model [19], [27], in which the vertical and horizontal extinction coefficients are different. Nonetheless, if such dependence on polarization is not strong, the simpler RVoG model can be employed, in which the extinction coefficient is polarization-independent. Given that the available input data of this article are dual-pol (not fully polarimetric), we only have access to a reduced observation space. Thus, we need to ignore the orientation effects in order to design a feasible inversion strategy. Consequently, the RVoG model will be used for inversion.

In the RVoG model, the only dependence of the coherence on polarization is found in the ground-to-volume ratio, which makes the coherences provided by the model to lie along a straight line on the complex plane. Derived from (10), the RVoG coherence as a straight line is expressed as

$$\tilde{\gamma}(\kappa_Z, \vec{w}) = e^{i\phi_{0_{\mathrm{D}}}} \left(\tilde{\gamma}_V + \frac{\mu_{\mathrm{D}}(\vec{w})}{1 + \mu_{\mathrm{D}}(\vec{w})} (1 - \tilde{\gamma}_V) \right) \tag{12}$$

as originally defined in [6], [18], and [24]. However, when the DB dominates the ground response and we work with a bistatic acquisition, the line equation derived from (11) results in

$$\tilde{\gamma}(\kappa_Z, \vec{w}) = e^{i\phi_{0_{\mathrm{DB}}}} \left(\tilde{\gamma}_V + \frac{\mu_{\mathrm{DB}}(\vec{w})}{1 + \mu_{\mathrm{DB}}(\vec{w})} (\gamma_{\mathrm{DB}} - \tilde{\gamma}_V) \right) \tag{13}$$

where γ_{DB} is the absolute value of the coherence for an infinite ground-to-volume ratio, instead of 1. This decrease in the coherence is a result of the differences in the travel paths of the DB contributions when returning to the receiving antennas, which is discussed in detail in [21] and [22]. The difference between the two cases is graphically shown in Fig. 2. Briefly, in the latter case, the point that defines the topographic phase is the intersection between the line and the circumference of radius γ_{DB}, instead of unit radius as in the normal case.

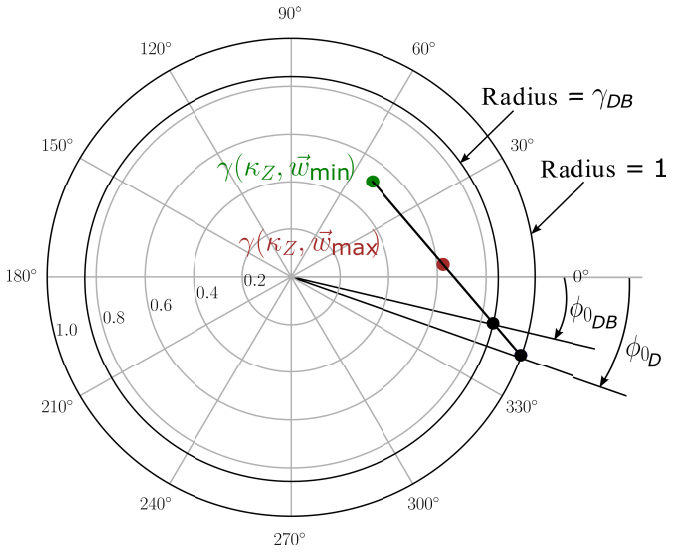

Fig. 2. Unit circle on the complex plane representing the extreme coherences, $\gamma(\kappa_Z, \vec{w}_{\mathrm{min}})$ (green dot) and $\gamma(\kappa_Z, \vec{w}_{\mathrm{max}})$ (red dot), and the line of the RVoG model when the DB ground contribution dominates (11).

III. PolInSAR Inversion Strategy

A. Inversion Algorithm

In the literature, one can find different strategies to retrieve the physical parameters of the scene employed in the RVoG model (see [8], [11], [14], [16]). Taking as reference [6] and [15], the methodology employed here particularizes the inversion procedure for the dual-pol TanDEM-X bistatic data, adapted to the specific properties of a scene in which the DB contribution dominates. The reader is advised to consult [6] and [15] for a broader explanation regarding the details of the algorithm. The inversion approach is summarized in Fig. 3. The algorithm is implemented in the python open-source code, which will be available in a public repository upon the publication of this manuscript. It consists of three main steps as follows.

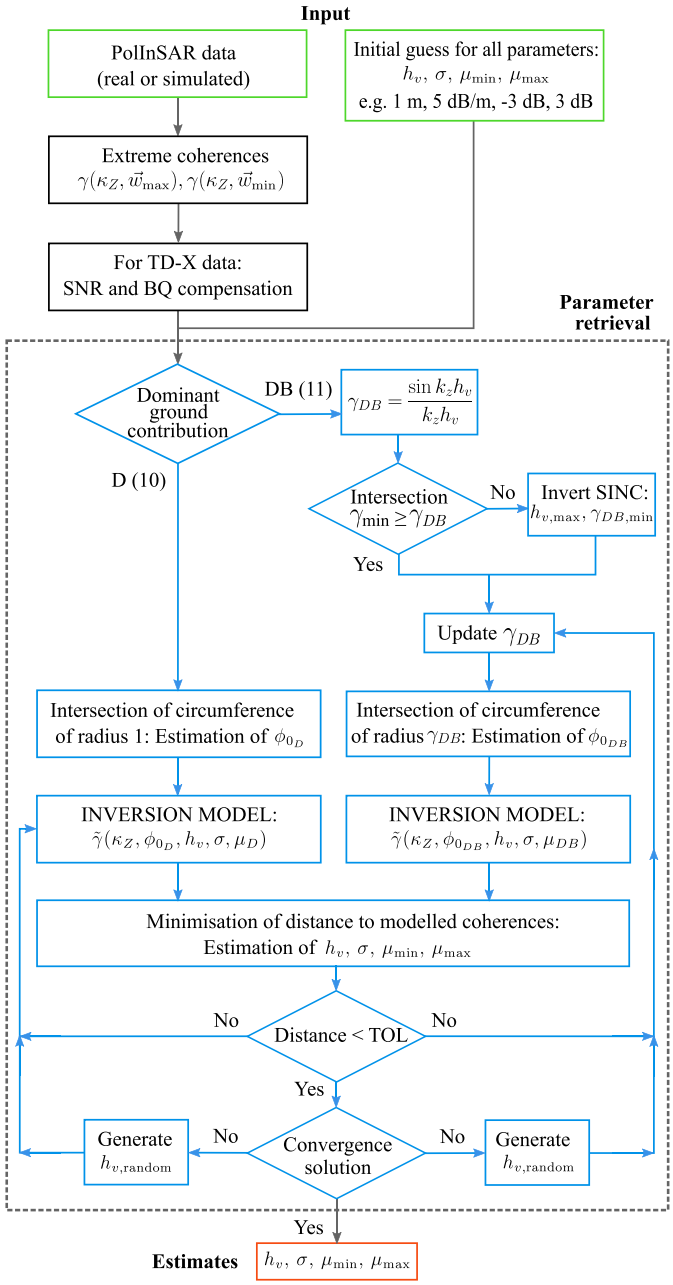

Fig. 3. Flow diagram of the proposed RVoG inversion approach for PolInSAR data and scenes characterized by a dominant DB ground contribution. The diagram describes the inversion procedure for a single PolInSAR model scene.

1) Line fit to the coherence region and selection of the coherences with minimum and maximum ground contributions, $\gamma(\kappa_Z, \vec{w}_{\min})$ and $\gamma(\kappa_Z, \vec{w}_{\max})$, hereafter called extreme coherences.
2) Compensation for the extreme coherences for all the nonvolumetric decorrelation terms: a) decorrelation due to thermal noise, which is defined by the signal-to-noise ratio (SNR) at each pixel, γ_{SNR} and b) decorrelation due to data quantization (BQ), γ_{BQ}.
3) Numerical estimation of the model parameters: topographic phase ϕ_0, vegetation height h_v, extinction σ, and two ground-to-volume amplitude ratios $\mu_{\min}$ and $\mu_{\max}$, one for each extreme coherence.

Steps 1) and 2) correspond to the ones defined in [15], so they are only briefly described here. As for the first step, among the different ways that exist to carry out the line fit to the coherences, i.e., [1], [20], [24], the proposed method implements the approach described in [6]. First, the border of the coherence region is generated, and then, the coherences with minimum and maximum phases are selected, thus defining the line shown in Fig. 2. The straight line generated by the ground-to-volume ratio $\mu(\vec{w})$ is the coherence region of the RVoG model, and the extreme coherences correspond to the ones with minimum and maximum ground contributions, $\gamma(\kappa_Z, \vec{w}_{\min})$ and $\gamma(\kappa_Z, \vec{w}_{\max})$, associated with the projection vectors $\vec{w}_{\min}$ and $\vec{w}_{\max}$, respectively.

Once the pair of extreme coherences is found, the second step is the correction of other nonvolumetric decorrelation terms, i.e., γ_{SNR} and γ_{BQ}, performed following the explanation given in [15]. After the extreme coherences are corrected, they are used as input to the third critical step: the parameter retrieval stage (gray dashed box in Fig. 3). At this point, coherence $\tilde{\gamma}$ is the only remaining term to be modeled according to the scattering properties of the scene.

Since the goal is to evaluate the effect of the DB decorrelation term present in bistatic acquisitions, in this article, the numerical estimation of the model parameters can be carried out in two ways: either considering a scene dominated by the direct ground contribution, and thus, coherence $\tilde{\gamma}$ is modeled according to (10); or considering a scene dominated by the DB contribution, where coherence $\tilde{\gamma}$ is modeled as in (11).

Regardless of the methodology selected, the estimation is performed by an iterative minimization in which the cost function is the distance between the measured extreme coherences $\gamma(\kappa_Z, \vec{w})$ and the modeled ones $\tilde{\gamma}$. The general expression for both methodologies is the following:

$$\min_{\phi_0, h_v, \sigma, \mu_{\max}, \mu_{\min}} \left\| \begin{bmatrix} \gamma(\kappa_Z, \vec{w}_{\max}) e^{-i\phi_0} \\ \gamma(\kappa_Z, \vec{w}_{\min}) e^{-i\phi_0} \end{bmatrix} - \begin{bmatrix} \tilde{\gamma}(\kappa_Z, \phi_0, h_v, \sigma, \mu_{\max}) \\ \tilde{\gamma}(\kappa_Z, \phi_0, h_v, \sigma, \mu_{\min}) \end{bmatrix} \right\| \quad (14)$$

where the minimum and maximum ground-to-volume ratios $\mu_{\min}$ and $\mu_{\max}$ are particularized to $\mu_{D,\min}$ and $\mu_{D,\max}$, or to $\mu_{DB,\min}$ and $\mu_{DB,\max}$, depending on the equation used for inversion, i.e., (10) or (11).

When the scene analyzed corresponds to a forest, the minimum ground-to-volume ratio can be assumed to be $\mu_{\text{D}}(\vec{w}_{\min}) = 0$ (see [6]). This assumption is usually satisfied for the forest scenes due to a negligible contribution coming from the ground compared with the contribution from the volume (i.e., tens of meters of vegetation height). However, when evaluating the crop scenes (i.e., with vegetation height from a few centimeters to a few meters), all polarimetric channels present some contribution from the ground, and hence, neither $\mu_{\text{D}}(\vec{w}_{\min})$ nor $\mu_{\text{DB}}(\vec{w}_{\min})$ can be assumed to be zero.

As depicted in Fig. 3, the first parameter to estimate is the ground phase ϕ_0. When the direct ground contribution dominates (10), the topographic phase is directly obtained by the crossing of the line defined by the RVoG model and

the unit circumference [see ϕ_{0_D} in Fig. 2 and (12)] [6], [18], [24]. Then, the remaining model parameters, i.e., h_v, σ, $\mu_{D,\max}$, and $\mu_{D,\min}$, are retrieved following the numerical minimization method in (14). In contrast, when the dominant ground contribution is the DB (11), the coherence of pure ground contribution ($\mu_{\mathrm{DB}} \rightarrow \infty$) decreases and the true topographic phase $\phi_{0_{\mathrm{DB}}}$ is defined by the crossing of the line with the circumference of radius γ_{DB} (13), as it is represented in Fig. 2. Therefore, the first effect of a wrong model selection is a bias in the estimation of ground topography, which, in turn, is expected to influence the estimation of the rest of the model parameters.

Since the extra decorrelation term γ_{DB} depends on the vegetation height h_v (8), which is one of the unknowns, the estimation of the topographic phase directly from the intersection between the line and the circumference is no longer fulfilled (i.e., the radius of the circumference is not known). This implies a series of additional considerations with respect to the conventional inversion of the RVoG model, which is further examined in the following section.

B. Parameter Retrieval in Bistatic Configurations With Dominant DB From the Ground

In the first place, not all the initial guesses of vegetation height (e.g., $h_v = 1$ m in a crop scenario) are valid, because the RVoG line (13) may not cross the circumference of radius γ_{DB} defined by that initial guess of h_v. Thus, prior to the numerical optimization, the input guess of the vegetation height needs to be checked for ensuring that the corresponding intersects the RVoG line, defined by the measured extreme coherences, at, at least, one point. With this purpose, the expression of the minimum coherence along the line $|\gamma_{\min}|$, derived in [24, eq. (7.49)], is reformulated here for the general case (valid for any two coherences), yielding

$$|\gamma_{\min}| = \frac{|\mathrm{Re}(\gamma_1)\mathrm{Im}(\gamma_2) - \mathrm{Im}(\gamma_1)\mathrm{Re}(\gamma_2)|}{|\gamma_1 - \gamma_2|} \tag{15}$$

where γ_1 and γ_2 correspond in practice to the coherences of the minimum and the maximum ground contribution $\gamma\left(\kappa_Z, \vec{w}_{\min}\right)$ and $\gamma\left(\kappa_Z, \vec{w}_{\max}\right)$, respectively (see Fig. 4).

Once $|\gamma_{\min}|$ is obtained from the extreme coherences, the maximum value of the vegetation height that can be used as the initial guess is limited by the $\sin c$ function in (8). Inverting the $\sin c$ function by means of a Taylor series expansion (see [24, eq. (5.57)]) using the first three terms leads to

$$x \ll 1 \Rightarrow \sin cx = \sum_{n=0}^{\infty} \frac{(-1)^n \cdot x^{2n}}{(2n+1)!} \approx 1 - \frac{x^2}{3!} + \frac{x^4}{5!}. \tag{16}$$

Then, combining (8), (9), and (16), the maximum or upper bound for the vegetation height, which needs to be considered for inversion, is obtained from the following expression:

$$h_{v,\max} \approx \frac{1}{\kappa_Z \sin^2\theta_0}\sqrt{10 - 60\sqrt{\frac{1}{36} - \frac{1-|\gamma_{\min}|}{30}}}. \tag{17}$$

Once the range of vegetation heights that assure the minimum coherence required to find a solution is constrained

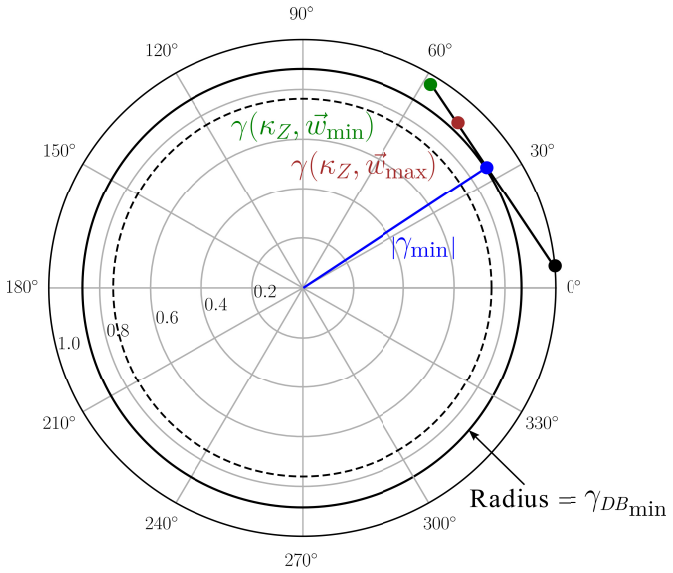

Fig. 4. Unit circle on the complex plane, representing the minimum coherence $|\gamma_{\min}|$ along the RVoG line when the DB ground contribution dominates (13). The dashed circumference corresponds to a radius γ_{DB} obtained with an invalid h_v guess (e.g., 1 m, for which there is no intersection with the line), whereas the continuous circumference is obtained from the value of h_v, which makes $|\gamma_{\min}| = \gamma_{\mathrm{DB}}$. Any value of h_v smaller than the one used for the continuous line (e.g., 0.5 m) would ensure the intersection between the line and the circumference.

(i.e., $|\gamma_{\min}| \leq |\gamma_{\mathrm{DB}}|$), an iterative solution search is implemented (see Fig. 3). We take first the value of vegetation height and obtain the corresponding γ_{DB}. Then, an initial value of $\phi_{0_{\mathrm{DB}}}$ is provided by the intersection of the line with the circumference of radius γ_{DB}. With $\phi_{0_{\mathrm{DB}}}$ and the initial guess of all model parameters (the selection strategy is discussed later in Section IV), the set (h_v, σ, $\mu_{\mathrm{DB},\max}$, $\mu_{\mathrm{DB},\min}$), which provides the minimum distance between the measured and modeled coherences, is estimated through (14). Here, a constrained minimization algorithm is employed, with a typical tolerance (TOL in Fig. 3) as the finalization condition. Next, γ_{DB} is updated with the estimated h_v, and the computation of the topographic phase $\phi_{0_{\mathrm{DB}}}$ and the minimization (14) are performed again. The iteration carries on until convergence to a solution with minimum distance between the measurements $\gamma\left(\kappa_Z, \vec{w}\right)$ and the model predictions $\tilde{\gamma}$.

Nevertheless, with the dual-pol single-baseline PolInSAR data, as the present case of study, the estimation of the RVoG parameters does not provide a unique solution but a range of possible solutions for which the numerical minimization in (14) is accomplished, since different combinations of model parameters produce similar model outputs. Consequently, the minimization in (14) might fall in local minima or simply provide an arbitrary solution that does not satisfy the condition of minimum distance. Here, as a reliable measure of convergence, the minimum distance that we have accepted as convergence criterion is 5% of the visible RVoG line length [i.e., the length of the segment from $\gamma\left(\kappa_Z, \vec{w}_{\min}\right)$ to $\gamma\left(\kappa_Z, \vec{w}_{\max}\right)$]. A relative measure of convergence is necessary in order to adapt the criterion to the input data. Since the inversion of the model is based on minimizing the distance

TABLE I
ACQUISITION SYSTEM PARAMETERS FOR THE CROP AND FOREST SCENARIOS

TanDEM-X system variables	Crops	Forests
Height of ambiguity HoA [m]	3 and 5	30 and 60
Vertical wavenumber κ_Z [rad/m]	2.1 and 1.2	0.2 and 0.1
Angle of incidence θ_0 [deg.]	20, 30, 40, 50	20, 30, 40, 50

TABLE II
SIMULATION INTERVALS OF THE PARAMETERS FOR THE CROP AND FOREST SCENARIOS

RVoG model parameters	Crops	Forests
Vegetation height h_v [m]	[0, $^{\text{HoA}}/_{2}$]	[2, $^{\text{HoA}}/_{2}$]
Extinction coefficient σ [dB/m]	[0, 10]	[0, 0.5]
Ground-to-volume ratios μ [dB]	[-10, 10]	[-10, 10]

TABLE III
CROP AND FOREST SCENARIOS: PARAMETER OPTIMIZATION CONSTRAINTS FOR INVERSION

Ranges of the optimisation constraints	
Vegetation height h_v [m]	[0, HoA]
Extinction coefficient σ [dB/m]	[0, 17]
Ground-to-volume ratios μ [dB]	[-20, 20]

between the coherences provided by the model and the data [see (14)], the minimum distance required to consider that convergence has been reached, which needs to be adapted to the separation among the data coherences. When they are quite separated, the convergence distance does not need to be as small as when they are very close together. Contrarily, e.g., when vegetation is very short, if all the possible coherences are located very close to a single point, the RVoG line from $\gamma(\kappa_Z, \vec{w}_{\text{min}})$ to $\gamma(\kappa_Z, \vec{w}_{\text{max}})$ is very short, and there is not much difference between them in absolute terms. Therefore, a single absolute magnitude does not ensure convergence in all cases. Numerous tests showed that all solutions fulfilling the condition of 5% of the RVoG line length provide the accuracy required to ensure satisfactory parameter estimations. When the resulting optimized solution does not converge to the established criterion, a different initial guess for the vegetation height (which in turn is known to be the most sensitive parameter [18], [19], [24], [28]) is generated randomly using a uniform distribution. The ranges in which the new guess is generated are the same as those we use to generate the simulated scenes (later specified in Section IV and Table II): $h_{v,\text{random}} \in [0, {}^{\text{HoA}}/_{2}]$ m for the crops and $h_{v,\text{random}} \in [2, {}^{\text{HoA}}/_{2}]$ m for the forests. In case the maximum vegetation height has been restricted [as in (17), i.e., the original guess of vegetation height did not provide a crossing with the circumference of radius γ_{DB}], the new vegetation height guess is generated accordingly, i.e., $h_{v,\text{random}} \in [0, h_{v,\text{max}}]$ m. The new value of h_v, together with the rest of the initial guesses for all the parameters, is taken as the input to a new iteration of the numerical estimation of the model parameters. The optimization process described above is, therefore, repeated for the same pixel until the solution fulfills the convergence distance.

IV. ANALYSIS WITH SIMULATED DATA

In this section, simulations are performed in order to assess the effect of the DB decorrelation term. Its influence on the inversion of the RVoG parameters as a function of both structural model parameters and system parameters is evaluated for two different scenarios: crops and forests. Table I shows the specific system configuration parameters of the TanDEM-X sensor, which have been selected for each scenario. The heights of ambiguity of 3 and 5 m (HoA $= {}^{2\pi}/_{\kappa_Z}$) are used for crops, while 30 and 60 m are employed for the forest scenes. In addition, each one of these baselines is tested at four angles of incidence, ranging from 20° to 50°.

At this point, it is worth mentioning that in sloped terrain with severe topography (e.g., forests in mountainous regions or crops in step farming), the influence of the local incidence angle on the model parameters should be considered. In the literature, one can find different strategies to deal with the terrain slope variation effect for the estimation of forest parameters [7], [29]–[31]. Positive slopes (i.e., facing toward the radar) decrease the local incidence angle and increase the vertical wavenumber. On the contrary, negative slopes (i.e., facing away from the radar) increase the local incidence angle and decrease the vertical wavenumber. Another direct consequence of a variation in the local incidence angle is a change in the ground-to-volume ratios. In forests, steep slopes facing the radar make the assumption of the null minimum ground-to-volume ratio (in at least one polarimetric channel) to break down, thus complicating the inversion methodology.

The intervals of the parameters used to generate the crop and forest scenarios are reported in Table II, whereas the optimization constraints, representing the intervals in which the possible solutions are searched for, are presented in Table III. Note that to ensure the feasible solutions and to avoid the edge effects, the bounds used as optimization constraints are beyond the margins employed to generate the simulated scenes. The upper bound of the height search space is set to HoA, and that of the extinction search space is equal to 17 dB/m (see the measurements in [32]).

The following simulation procedure is conducted for the evaluation of the influence of the DB on the inversion of the scene parameters. Each possible combination of the system and scene parameters generates a pair of theoretical coherences, $\gamma(\kappa_Z, \vec{w}_{\text{min}})$ and $\gamma(\kappa_Z, \vec{w}_{\text{max}})$, which are provided by the forward model through either (10) or (11). These simulated coherences are the input to the numerical inversion. For every scene (i.e., every pair of theoretical coherences), the model is inverted employing a first set of initial guesses with the average values of each variable, e.g., $h_v = 1$ and 10 m, $\sigma = 5$ and 0.25 dB/m (for crops and forests, respectively), $\mu_{\text{min}} = -3$ dB, and $\mu_{\text{max}} = 3$ dB [32]. In the end, the optimized solutions that satisfy the convergence criterion are saved for their later analysis.

Even in the case of data acquired in the monostatic mode or when there is a dominant direct ground contribution and

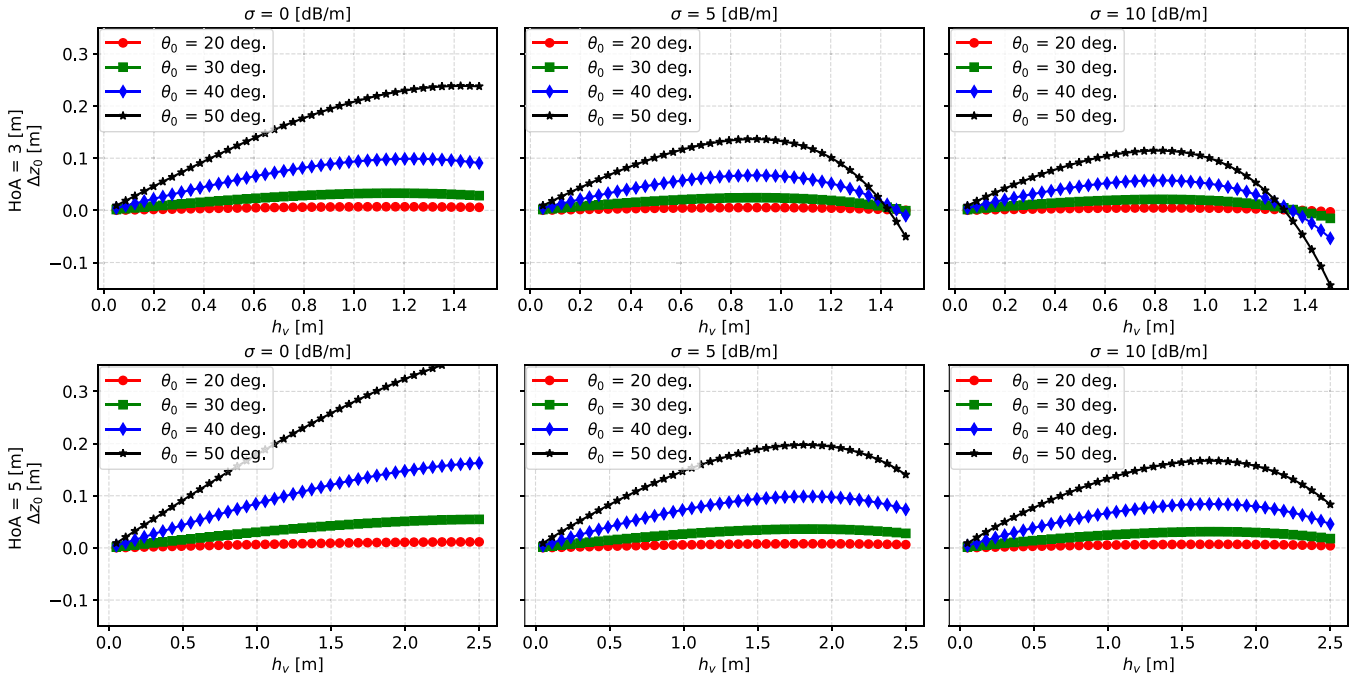

Fig. 5. Topographic error Δz_0 obtained as a function of the vegetation height for four incidence angles. The first row corresponds to the error for HoA = 3 m ($\kappa_Z = 2.1$ rad/m), whereas the second row to HoA = 5 m ($\kappa_Z = 1.25$ rad/m). Each column represents the error obtained for $\sigma = 0$, 5, and 10 dB/m, respectively. Ground-to-volume ratios are $\mu_{\min} = -3$ dB and $\mu_{\max} = 3$ dB.

not a DB one, the inversion of the RVoG model is expected to not perform ideally due to a lack of sensitivity for very short heights and to other numerical limitations related to optimization. Thus, the errors originated by the DB must be clearly separated from the intrinsic errors that would appear also in its absence. For this reason, three methodologies have been compared to quantify properly the effect of the DB decorrelation term. The first methodology assumes a scenario with a dominant direct ground contribution, and thus, it applies (10) to both forward model and inversion. In the second methodology, the forward model corresponds to a dominant DB ground contribution (11), but the inversion ignores it and employs (10). Finally, the third methodology acknowledges the presence of a dominant DB ground contribution, and both forward model and inversion make use of (11). In the following, for the sake of interpretation, the first methodology will be referred to as D-D, the second as DB-D, and the third as DB-DB.

To measure the performance of inversion, the results are presented in terms of the absolute error

$$\Delta x = x_{\text{estimated}} - x_{\text{true}}. \tag{18}$$

In addition, the relative mean error (RME [%]) is calculated as

$$\text{RME} = \frac{x_{\text{estimated}} - x_{\text{true}}}{x_{\text{true}}} \cdot 100 = \frac{\Delta x}{x_{\text{true}}} \cdot 100 \tag{19}$$

where $x_{\text{estimated}}$ corresponds to the estimate and x_{true} corresponds to the parameter of the simulated scene using the forward RVoG model.

The errors obtained in the estimation of topography, vegetation height, extinction, and ground-to-volume ratios are presented and analyzed in Sections IV-A and IV-B for the crop and forest scenarios, respectively.

A. Crop Scenario

1) Topography: As the flow diagram of the proposed inversion approach indicates (see Fig. 3), the topographic phase is the first parameter to be estimated [2]. Therefore, we analyze in the first place the error produced in the retrieval of the topographic phase in the case illustrated in Fig. 2, when data correspond to a scene with a dominant DB ground contribution (11), but the inversion assumes a dominant direct ground contribution (10). The phase error is defined as

$$\Delta\phi_0 = \phi_{0_{\text{DB}}} - \phi_{0_{\text{D}}} \tag{20}$$

and is translated into the topography error as

$$\Delta z_0 = \Delta\phi_0 / \kappa_Z. \tag{21}$$

Fig. 5 represents the topographic error Δz_0 obtained for a range of vegetation heights h_v and for four incidence angles (see Table I). Moreover, since the estimation accuracy of the RVoG model inversion depends on the effective baseline κ_Z and on the available interferometric coherence [7], [33], the results are computed for the heights of ambiguity of 3 and 5 m, which correspond to $\kappa_Z = 2.1$ and 1.2 rad/m, respectively. The results are presented for null, medium (i.e., 5 dB/m), and high (i.e., 10 dB/m) extinctions.

The first aspect that can be observed is that for steep incidence angles, the bias is very small or negligible. In the worst case, for $\sigma = 0$ dB/m, the error is less than 1 cm at 20° and less than 4 cm at 30°. The reason of this dependence on the incidence angle is the conversion factor

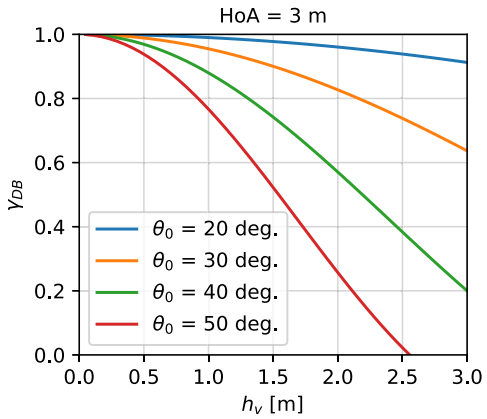

Fig. 6. Comparison of the DB decorrelation term as a function of the vegetation height for HoA = 3 m.

between κ_Z and k_z, explained in (8) and (9). The strong influence of the incidence angle on γ_{DB} is reflected in $\gamma_{\mathrm{DB}} = (\sin(\kappa_Z \cdot \sin^2\theta_0 \cdot h_v))/(\kappa_Z \cdot \sin^2\theta_0 \cdot h_v)$, where the sine of the incidence angle appears to the square. This means that steep incidences (i.e., 20°) turn into γ_{DB} values close to 1, whereas shallow incidences (i.e., 50°) make γ_{DB} to decrease rapidly. When $\gamma_{\mathrm{DB}} \simeq 1$, there is almost no DB decorrelation, and the coherences on the complex plane are very close to the monostatic configuration (see Fig. 2). In these situations, the effect of the DB factor is insignificant. Nevertheless, for shallower incidence angles, e.g., 40° and 50°, there is a clear bias that is expected to affect the estimation of the rest of model parameters. This error is greater for low extinctions and higher heights of ambiguity, and it increases for larger values of height, since as the vegetation height increases, γ_{DB} (8) decreases, and the circumference that fixes the topographic phase shrinks. Fig. 6 illustrates how γ_{DB} decreases with increasing h_v at the four different incidence angles. Thus, with $\sigma = 0$ dB/m and HoA = 3 m, the topographic error reaches 10 cm at 40° and 24 cm at 50°, for vegetation heights around 1.4 m. For the same extinction and HoA = 5 m, the maximum errors move to the largest heights (i.e., 2.5 m), with the values of 16 and 37 cm at 40° and 50° (i.e., relative errors around 7% and 15%), respectively.

On the other hand, there is a second trend in the plots shown in Fig. 5 in which, from a certain height and for high extinctions, the error is first canceled, and then, the topography starts to be underestimated. The maximum error corresponds to a relative error of 6% in the worst case, with HoA = 3 m, $\sigma = 10$ dB/m, and $h_v = 1.5$ m. Such a cancellation of the topography error takes place when the RVoG line exhibits a radial arrangement on the complex plane, and hence, the topographic phase coincides with the two expressions (10) and (11).

2) Vegetation Height: Fig. 7 compares the error obtained in the vegetation height estimates applying the RVoG model following the methodology described in Section III for the cases D-D, DB-D, and DB-DB. Therefore, the left and right columns correspond to the cases in which the same expression is used for the forward model and the inversion, whereas the central column corresponds to the case of ignoring the DB effect in the inversion but with data generated in its presence. The error is calculated in absolute terms following (18), particularized for the vegetation height. The results are presented as a function of height and extinction within the intervals [0, 1.5] m and [0, 10] dB/m (see Table II), respectively. The ground-to-volume ratios of the two channels are fixed to the values $\mu_{\min} = -3$ dB and $\mu_{\max} = 3$ dB. With respect to the acquisition system parameters (see Table I), the selected spatial baseline for this test is $\kappa_Z = 2.1$ rad/m (i.e., HoA = 3 m), and the extreme look angles that we have chosen are 20° and 50°.

A common behavior in the three cases is the error present when height is above 80 cm and the extinction is either low or high. For this range of values, there is a deviation between the real and estimated values that, in the worst case, reaches 10 cm approximately. This pattern is repeated for all the angles of incidence in the methodologies D-D and DB-DB, which are very similar. The fact that this error occurs even when the scene is properly characterized (i.e., cases D-D and DB-DB) means that its origin is not the DB decorrelation but the RVoG model inversion itself.

As expected from the previous analysis of the topographic error, which corresponds to the DB-D case, there is an evident increase in the influence of the DB decorrelation term when one moves to shallower incidence angles. This influence is translated into a greater error when the DB is ignored in the inversion. Due to the dependence of γ_{DB} on the product $k_z h_v$ [see (8) and (9)], only by acknowledging it in the inversion, the RVoG model constrains the vegetation height according to the baseline κ_Z and the angle of incidence θ_0. Thus, the maximum relative error in the case DB-D for a look angle of 50° is 25% around a vegetation height of 80 cm. In contrast, this overestimation is compensated when the inversion model does consider the DB term (case DB-DB).

A detailed insight into the effect of ignoring the DB in the inversion of vegetation height is presented in Fig. 8. The difference between the estimates following the methodologies DB-D and DB-DB is presented, named $\Delta h_{v,\text{D-DB}}$. The results are plotted for 50°, when the overestimation is most significant. The area that encompasses the higher possible errors is found for the values of h_v from 50 cm to 1.3 m, approximately. As shown in the case DB-D in Fig. 7 for 50°, the greatest absolute errors occur at high vegetation heights and extinctions. However, the maximum relative errors when the scene has been wrongly characterized are located at the average values of the scene height, which is normally the region of greatest interest in terms of inversion accuracy. The maximum error is 8 cm (around 10%), when $h_v = 76$ cm and $\sigma = 0.67$ dB/m.

3) Extinction Coefficient: Fig. 9 presents the absolute error (18) in the estimates of the extinction coefficient for the three methodologies compared: D-D, DB-D, and DB-DB. The main difference with respect to the estimation of the vegetation height is that the error for the extinction coefficient is considerably larger, ranging from −3 to 3 dB/m, underestimating the high values and overestimating the low values. Furthermore, the error profile remains almost constant as a function of vegetation height, which suggests that the

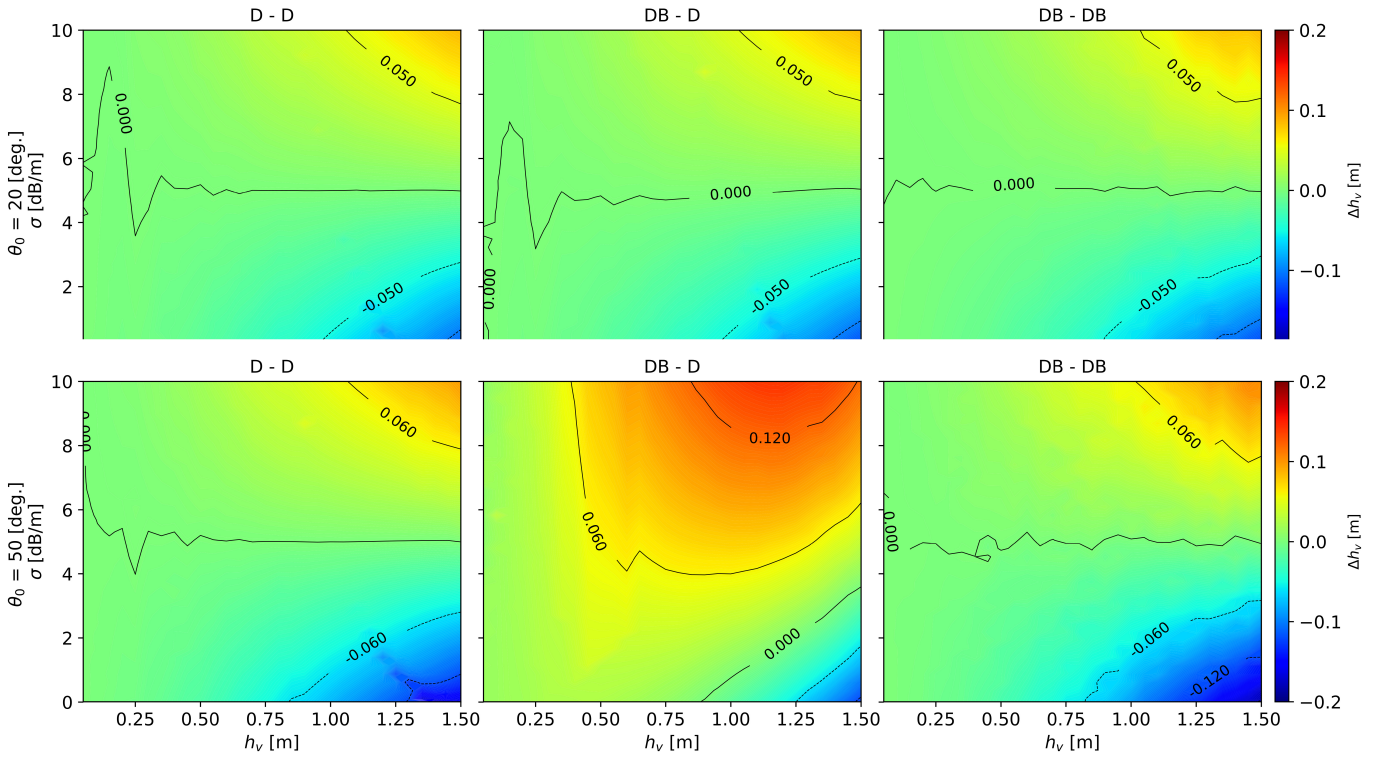

Fig. 7. Vegetation height error obtained with the method described in Section III-A. Model parameters: $h_v \in [0, 1.5]$ m, $\sigma \in [0, 10]$ dB/m, $\mu_{\min} = -3$ dB, and $\mu_{\max} = 3$ dB. Other system parameters: $\theta_0 = 20°$ and $50°$, and HoA = 3 m. (Left) Methodology D-D. (Middle) Methodology DB-D. (Right) Methodology DB-DB.

extinction estimation is relatively insensitive to the changes in the vegetation height.

On the other hand, several analogies are found with prior evaluations (see Sections IV-A1 and IV-A2). The error in extinction at 20° is roughly the same one whether the DB is considered in the inversion or not, whereas at 50°, the results of the DB-D methodology show a clear overestimation in comparison with the other ones, D-D and DB-DB.

The large error that the DB-D case exhibits for 50° and short vegetation heights is also visible for 20° in the methodologies D-D and DB-D, in contrast to what the vegetation height estimates reflect (see Fig. 7). For vegetation height values below 30 cm, approximately, the overestimation is caused by a lack of interferometric sensitivity (as demonstrated in [34]). This is a limitation due to the baseline, since for short vegetation, the product of height and vertical wavenumber ($h_v k_z$) is very small, which means that there is not sufficient interferometric sensitivity to the vertical distribution of the scatterers in the scene. Albeit this overestimation is constrained to short values of h_v, the dependence of the DB factor γ_{DB} on the incidence angle [see (8) and (9)] explains the greater bias for 50° when the inversion ignores it (case DB-D). Comparing the three methodologies, the results indicate that this error is mostly counteracted when the model used for inversion goes in accordance with the scene simulated, as in the cases D-D and DB-DB.

The influence of the initial guess of extinction needs to be discussed at this point. The results shown in Fig. 9 are obtained

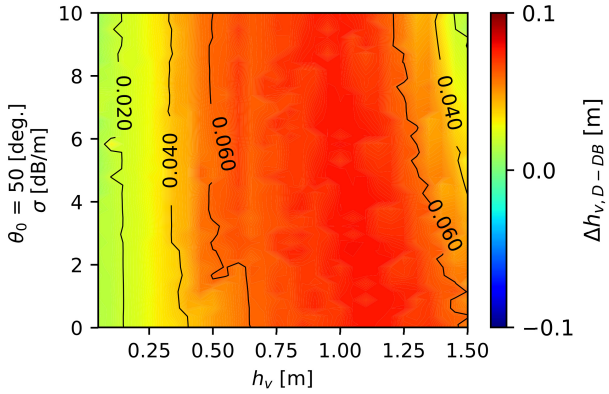

Fig. 8. Vegetation height overestimation of the case DB-D with respect to the case DB-DB. Results obtained using the method described in Section III-A. Model parameters: $h_v \in [0, 1.5]$ m, $\sigma \in [0, 10]$ dB/m, $\mu_{\min} = -3$ dB, and $\mu_{\max} = 3$ dB. Other system parameters: $\theta_0 = 50°$ and HoA = 3 m.

with an average value for the initial guess: 5 dB/m. In the cases D-D and DB-DB, as well as for the steep incidences in the case DB-D, there is a null estimation error around this value, whereas there is an underestimation for higher values and an overestimation for lower values. Additional tests with higher and lower values of initial guess show that the output estimates fluctuate around the input value, regardless of its magnitude. Therefore, in general, the resulting extinctions could not be considered as valid estimates. This is demonstrated in Fig. 10 (first row), where the results of

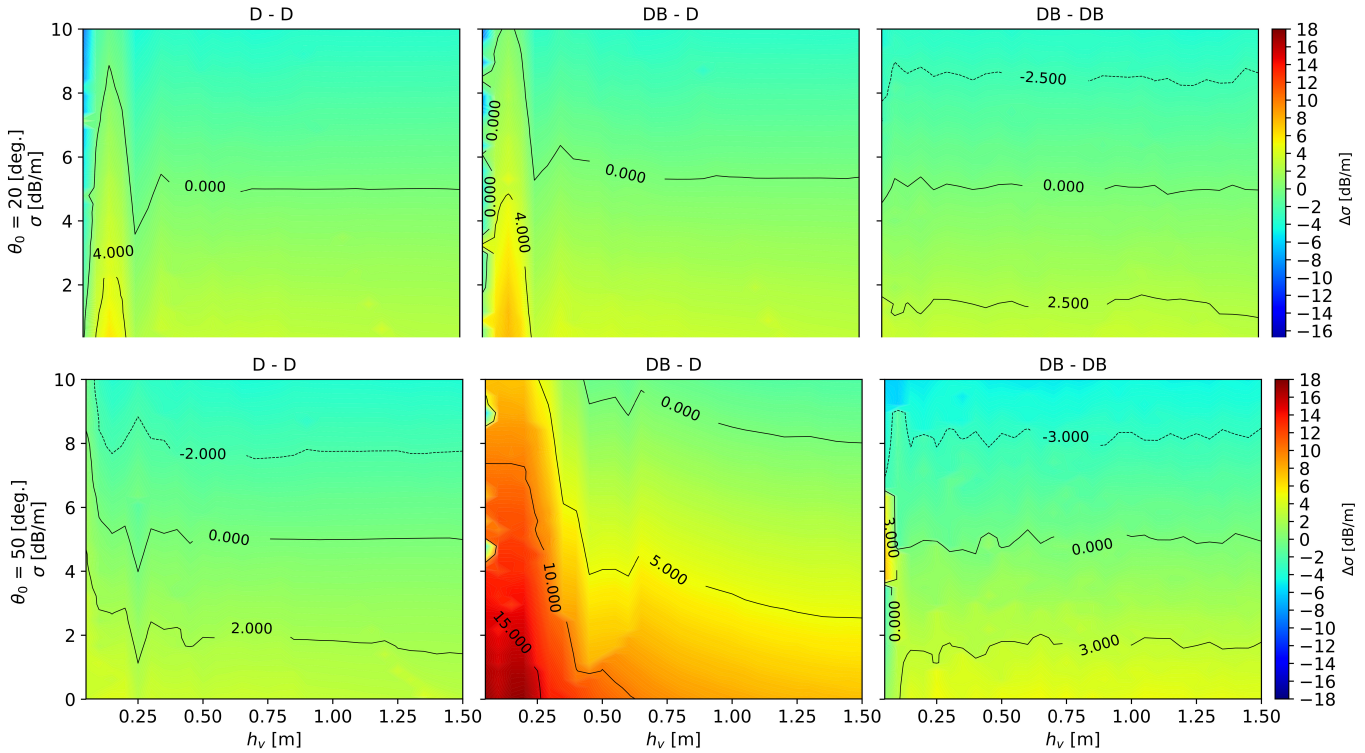

Fig. 9. Extinction error obtained with the method described in Section III-A. Model parameters: $h_v \in [0, 1.5]$ m, $\sigma \in [0, 10]$ dB/m, $\mu_{\min} = -3$ dB, and $\mu_{\max} = 3$ dB. Other system parameters: $\theta_0 = 20°$ and $50°$, and HoA $= 3$ m. (Left) Methodology D-D. (Middle) Methodology DB-D. (Right) Methodology DB-DB.

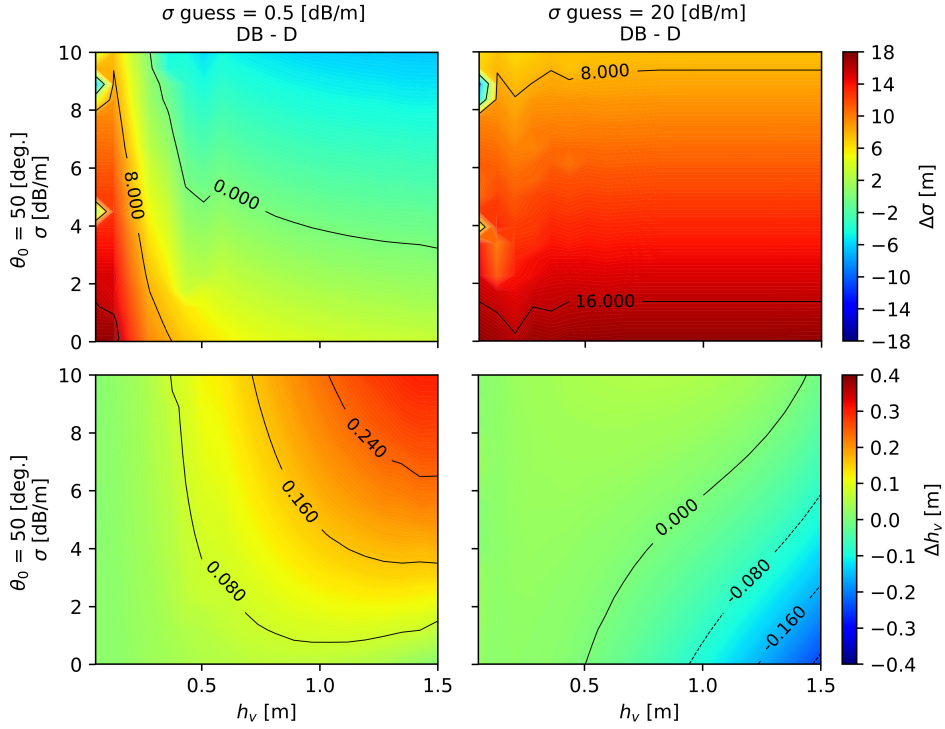

Fig. 10. (First row) Extinction error and (Second row) Vegetation height error using as initial guess (Left) $\sigma = 0.5$ dB/m and (Right) $\sigma = 20$ dB/m. Model parameters: $h_v \in [0, 1.5]$ m, $\sigma \in [0, 10]$ dB/m, $\mu_{\min} = -3$ dB, and $\mu_{\max} = 3$ dB. Other system parameters: $\theta_0 = 50°$, and HoA $= 3$ m.

the extinction estimates using as initial guess $\sigma = 0.5$ and 20 dB/m are shown. The results are presented for the worst case, i.e., following methodology DB-D for $\theta_0 = 50°$.

The consequence of this insensitivity to extinction is that varying the initial guess affects the estimation of the rest of model parameters, i.e., vegetation height and

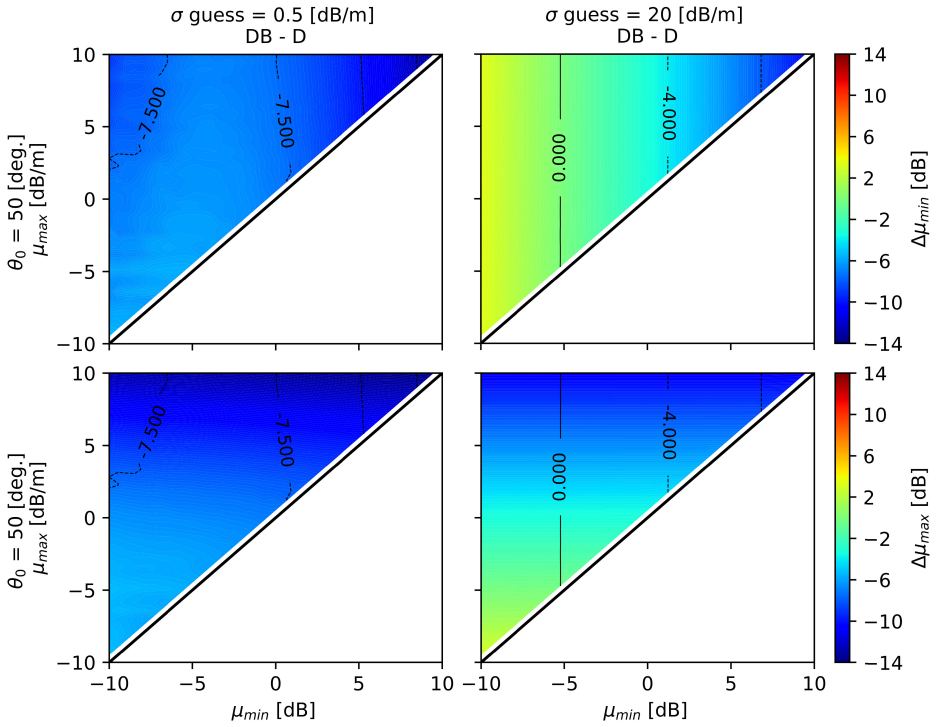

Fig. 11. (First row) Minimum ground-to-volume ratio error and (Second row) maximum ground-to-volume ratio error using as initial guess (Left) $\sigma = 0.5$ dB/m and (Right) $\sigma = 20$ dB/m. Model parameters: $h_v \in [0, 1.5]$ m, $\sigma \in [0, 10]$ dB/m, $\mu_{\min} = -3$ dB, and $\mu_{\max} = 3$ dB. Other system parameters: $\theta_0 = 50°$ and HoA = 3 m.

ground-to-volume ratios. The results of the vegetation height estimates are shown in Fig. 10 (second row). A low initial guess for extinction is translated into an overestimation of height for $h_v > 1$ m and $\sigma > 5$ dB/m (see the top-right corner of the plots in Fig. 7). On the contrary, a high initial guess for extinction produces an underestimation of height for $h_v > 1$ m and $\sigma < 5$ dB/m (see the bottom-right corner of the plots in Fig. 7). As for the ground-to-volume ratios (see Fig. 11), which are analyzed in the next section, for a fixed $h_v = 1$ m and $\sigma = 5$ dB/m, considering as the initial guess a low value of extinction increases considerably the error, leading to an overall underestimation. Under the same conditions, the inversion using a high initial value of extinction results in an overestimation of low ground-to-volume ratio pairs and an underestimation of high ground-to-volume ratio pairs. In these situations, the error caused by ignoring the DB in the inversion is mixed with the error of underestimating or overestimating the extinction.

4) Ground-to-Volume Ratios: The evaluation of the ground-to-volume ratios, corresponding to the minimum and maximum ground contributions, is displayed in Figs. 12 and 13, respectively. Similar to previous assessments, the error analysis is performed over the average values of the model parameters. Namely, vegetation height and extinction are fixed to values $h_v = 1$ m and $\sigma = 5$ dB/m. The ground-to-volume ratios are simulated within the interval $[-10, 10]$ dB under the condition $\mu_{\max} > \mu_{\min}$ in order to ensure the physically meaningful solutions.

There are evident similarities when comparing the estimates of both magnitudes. Once again, the error of ignoring the DB contribution (see the case DB-D) can be neglected for the steep angles of incidence (20°), and it should be considered for shallower incidence angles, such as 50°. For this latter θ_0, the maximum underestimation is found for the highest pair of simulated ground-to-volume ratios (i.e., $\mu_{\min} = 9.5$ dB and $\mu_{\max} = 10$ dB), and it is around 8 dB.

On the lower values of the simulations (i.e., bottom-left corner of Figs. 12 and 13), there is an overestimation, which is more noticeable in the $\mu_{\min}$ estimates. A maximum deviation is found at values $\mu_{\min} = -10$ dB and $\mu_{\max} = -9.5$ dB along the three cases evaluated for 20°, and even in the case D-D for 50°. This is explained by the fact that such low values of ground-to-volume ratios mean that the backscattering contribution from the ground is insignificant compared with the contribution from the volume. Under these circumstances, the scattering is concentrated in a single point at the top of the vegetation layer. The RVoG line on the complex plane shortens, and the extreme phases associated with the polarization states $\vec{w}_{\min}$ and $\vec{w}_{\max}$ are very similar to each other and far away from the topographic phase. Therefore, the variability of the possible solutions increases. This scenario complicates the retrieval of the topographic phase, and thus the retrieval of the rest of the model parameters.

Observing the estimates of the methodology DB-DB for 50°, one can note how the inclusion of the DB term in the inversion compensates considerably the error in both ground-to-volume ratios. Not only the underestimation at high ground-to-volume pairs is corrected but also the overestimation that appears at the low pairs of simulated ground-to-volume ratios (which is present in the case D-D).

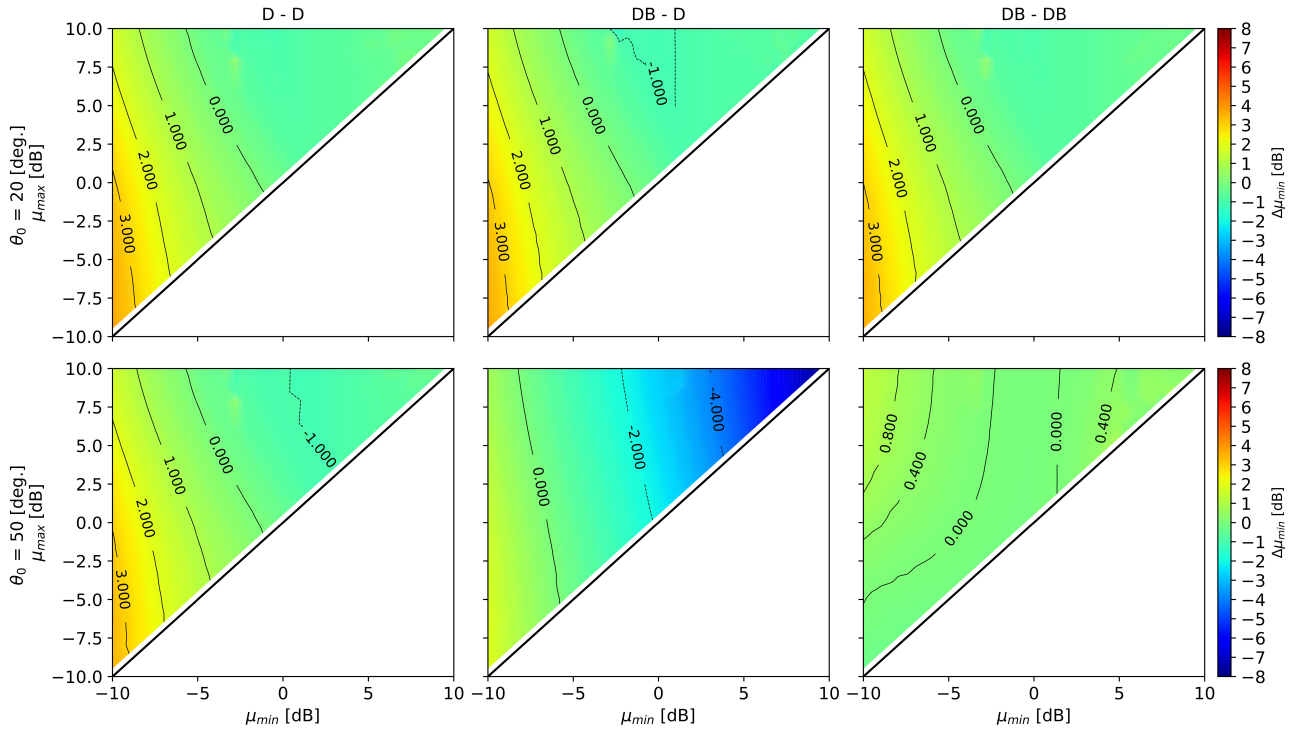

Fig. 12. Error in the minimum ground-to-volume ratio estimated with the method described in Section III-A. Model parameters: $h_v = 1$ m, $\sigma = 5$ dB/m, $\mu_{\min} \in [-10, 10]$ dB, and $\mu_{\max} \in= [-10, 10]$ dB. Other system parameters: $\theta_0 = 20°$ and $50°$, and HoA $= 3$ m. (Left) Methodology D-D. (Middle) Methodology DB-D. (Right) Methodology DB-DB.

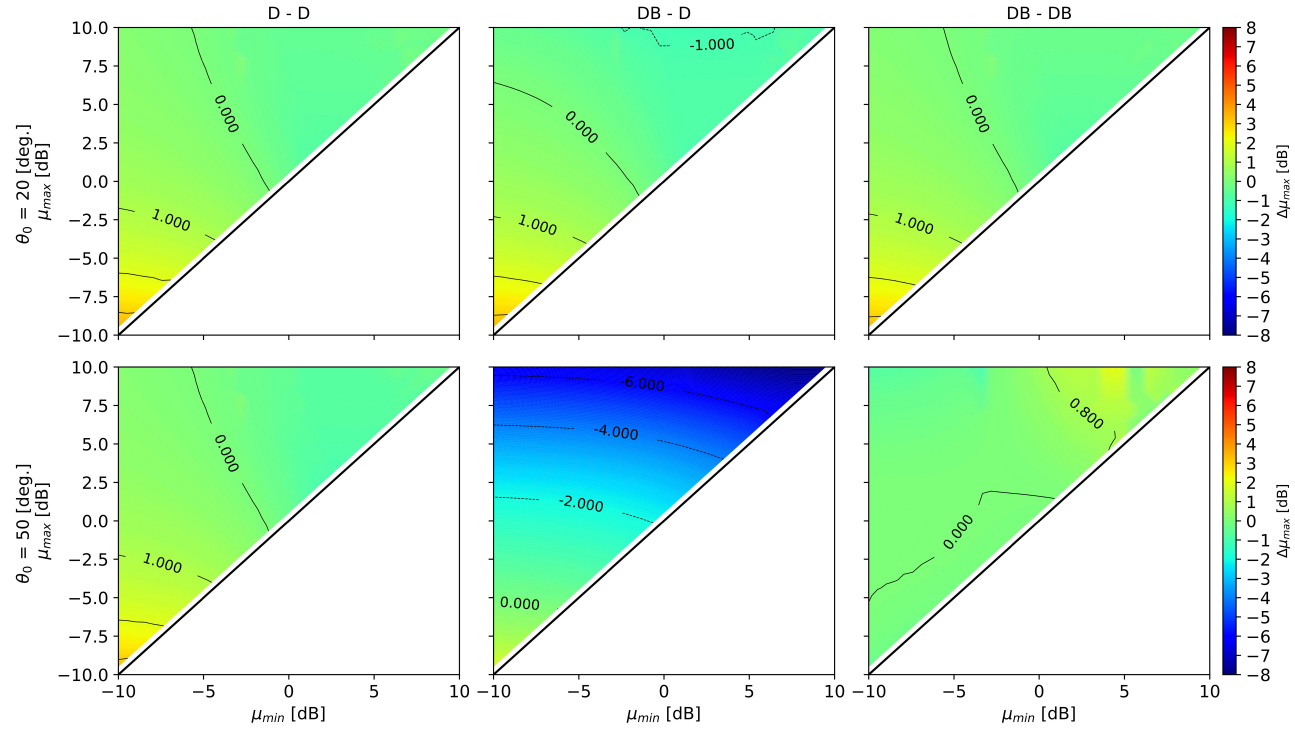

Fig. 13. Error in the maximum ground-to-volume ratio estimated using the method described in Section III-A. Model parameters: $h_v = 1$ m, $\sigma = 5$ dB/m, $\mu_{\min} \in [-10, 10]$ dB, and $\mu_{\max} \in= [-10, 10]$ dB. Other system parameters: $\theta_0 = 20°$ and $50°$, and HoA $= 3$ m. (Left) Methodology D-D. (Middle) Methodology DB-D. (Right) Methodology DB-DB.

In summary, in crop scenarios, we have seen that the DB decorrelation term needs to be considered in the parameter retrieval when we work with oblique incidences, but it is not necessary for steep angles. Vegetation height and ground-to-volume ratios are well estimated when the DB is ignored, but the incidence angle is steep, whereas for shallow angles,

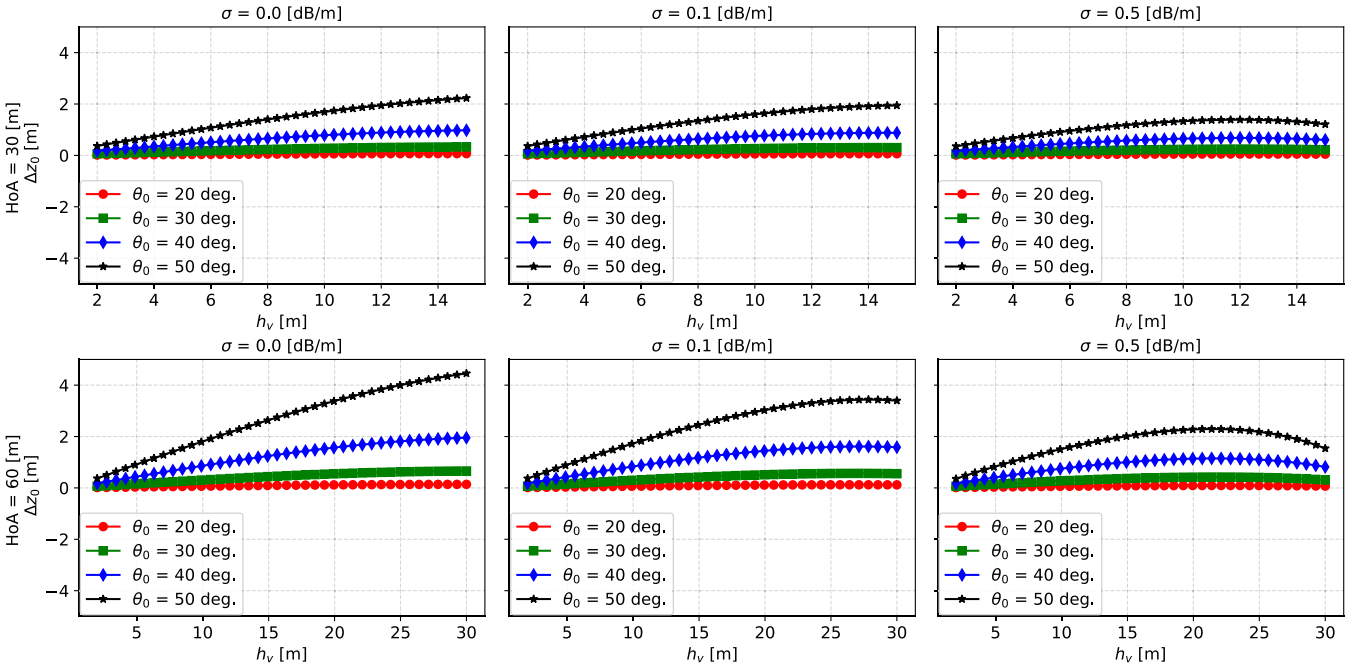

Fig. 14. Topographic phase error Δz_0 obtained as a function of the vegetation height for four incidence angles. The first row corresponds to the error for HoA = 30 m ($\kappa_Z = 0.2$ rad/m), whereas the second row to HoA = 60 m ($\kappa_Z = 0.1$ rad/m). Each column represents the error obtained for $\sigma = 0$, 0.1, and 0.5 dB/m, respectively. The ground-to-volume ratios are $\mu_{\min} = -3$ dB and $\mu_{\max} = 3$ dB.

the DB term needs to be considered in the inversion to provide good estimates. Regarding the extinction, its estimation is not reliable in any case (i.e., considering or not the DB), since it clearly depends on the initial guess. In the context of simulations, a wrong extinction estimation affects the reliability of the other parameters. Hence, an average extinction as the initial guess for the inversion has been employed for separating the effect of the DB in the estimates with respect to the effect of the initial guess of extinction.

B. Forest Scenario

1) Topography: Analogous to Section IV-A1, this section quantifies the topographic error over the forest scenario, defined as (20) and (21), and illustrated in Fig. 14.

The error Δz_0 is calculated for a range of vegetation heights h_v adapted to the size of the forests (see Table II), and hence to the corresponding baselines as well, i.e., $\kappa_Z = 0.2$ and 0.1 rad/s (see Table I). In the literature, typical extinction values employed for forests are around 0–0.5 dB/m [7]. Therefore, the error is here presented for $\sigma = 0$, 0.1, and 0.5 dB/m.

Fig. 14 highlights that the results retrieved in the agricultural scenario can be extrapolated to forests, considering the proportional increase that implies dealing with the vegetation height values of greater magnitude. In particular, the first trend that one can perceive is that the bias is insignificant for steep incidence angles, and it increases for more oblique ones (see Fig. 15 for a graphical explanation). In the worst case, for a fixed $\sigma = 0$ dB/m and HoA = 30 m, the topographic error is less than 7 cm for 20° and below 33 cm for 30°. Likewise, the second trend is that the topographic mismatch

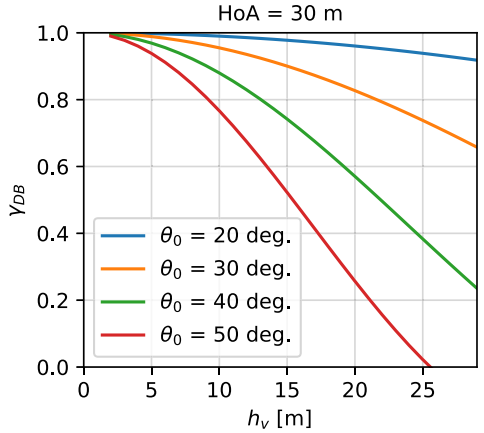

Fig. 15. Comparison of the DB decorrelation term as a function of the vegetation height for HoA = 30 m.

between the estimations and the measurements is greater for low values of extinction (i.e., 0 dB/m) and higher heights of ambiguity (i.e., 60 m). Thus, the maximum errors for HoA = 30 and 60 m, are found for $\sigma = 0$ dB/m at the greatest height simulated: 2.2 m of error at 15 m for HoA = 30 m and 4.3 m at 30 m for HoA = 60 m, which represent the relative errors around 15% in both cases.

The role of HoA in the estimation of all parameters is twofold. On the one hand, it acts as a scaling factor, as it can be deduced from the topography estimation shown in Fig. 14 and is well explained in [31]. A forest scenario evaluated with smaller values of HoA is expected to suffer from smaller estimation errors, because a larger spatial baseline is available, which implies a higher interferometric sensitivity (i.e., greater

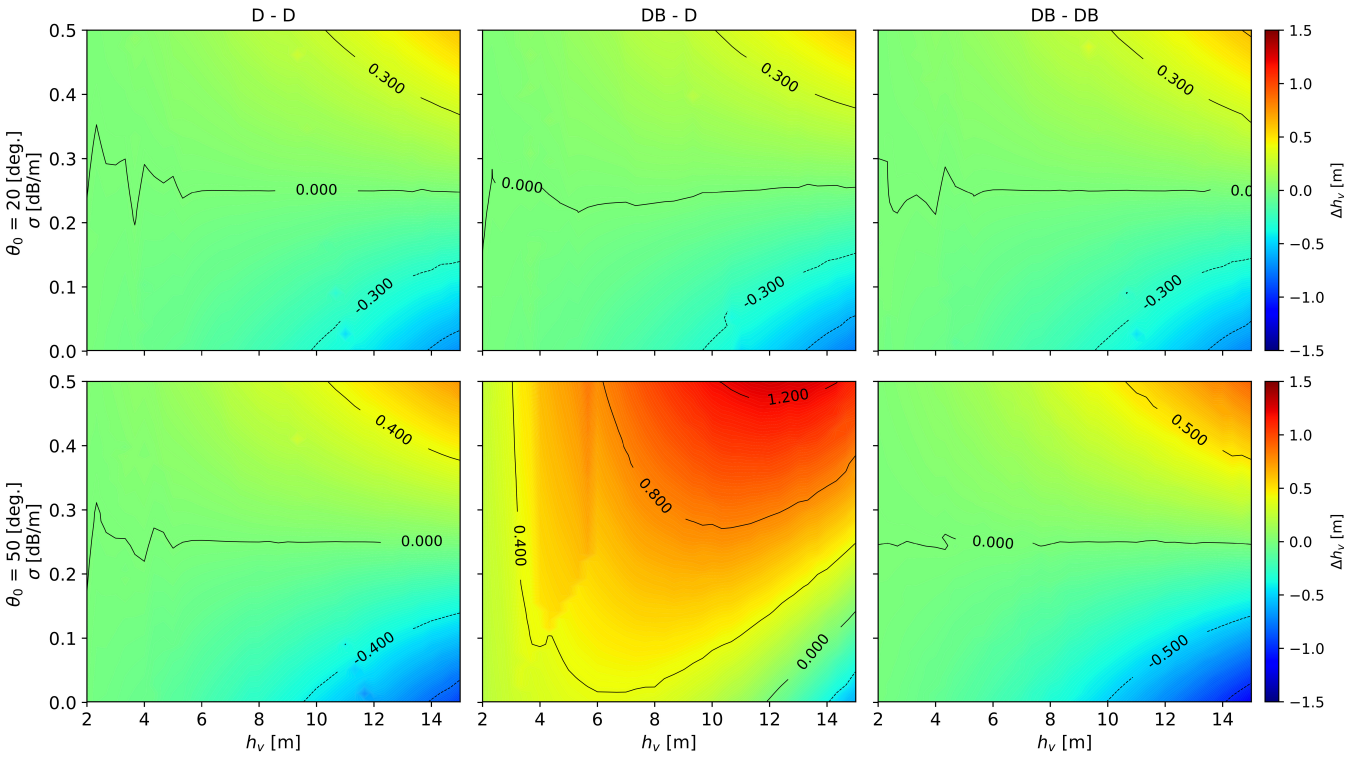

Fig. 16. Vegetation height error obtained using the method described in Section III-A. Model parameters: $h_v \in [2, 15]$ m, $\sigma \in [0, 0.5]$ dB/m, $\mu_{\min} = -3$ dB, and $\mu_{\max} = 3$ dB. Other system parameters: $\theta_0 = 20°$ and $50°$, and HoA $= 30$ m. (Left) Methodology D-D. (Middle) Methodology DB-D. (Right) Methodology DB-DB.

sensitivity to the RVoG parameters translates into a higher accuracy of the estimates). Unfortunately, in practice, decreasing the HoA entails two problems: the maximum vegetation height that can be retrieved is also decreased in the same proportion (hence leaving out areas with tall trees that could be considered with larger HoA) and a stronger range filtering needs to be applied in the preprocessing for compensating the increased wavenumber shift (hence degrading the spatial resolution in range).

The last trend, which is also common to both crops and forests, is that for a specific height and increasing extinction, the resulting Δz_0 starts to decrease and then becomes null (i.e., the RVoG line is radial on the complex plane).

2) Vegetation Height: In Fig. 16, Δh_v is plotted for HoA $= 30$ m and $\kappa_Z = 0.2$ rad/m as a function of height and extinction within the ranges [2, 15] m and [0, 0.5] dB/m, respectively (see Table II). To be consistent with the precedent assessments, the rest of the parameters are the same as the ones employed in Section IV-A2.

As anticipated by the previous results, the performance of the inversion algorithm is not likely to be affected by the DB factor for incidence angles steeper than 30°. For 20°, the first row of Fig. 16 confirms that there is no evident difference among the results of the three methodologies. On the contrary, a visible overestimation arises when the γ_{DB} factor is overlooked in the inversion for shallower incidence angles, as shown in the case DB-D for 50°. In relative terms, the greatest overestimation caused by ignoring this factor in

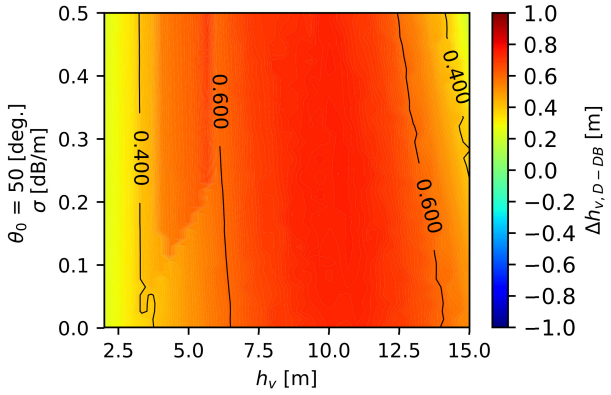

Fig. 17. Vegetation height overestimation of case DB-D with respect to the case DB-DB. Results obtained using the method described in Section III-A. Model parameters: $h_v \in [0, 15]$ m, $\sigma \in [0, 0.5]$ dB/m, $\mu_{\min} = -3$ dB, and $\mu_{\max} = 3$ dB. Other system parameters: $\theta_0 = 50°$ and HoA $= 30$ m.

the inversion is found at low values of vegetation height and large values of extinction (for $\theta_0 = 50°$), reaching a maximum deviation around 16% at $h_v = 4$–6 m and σ above 0.3 dB/m. However, for average values of these parameters (i.e., h_v around 8 m and σ around [0.1, 0.3] dB/m, approximately), such an overestimation remains below 10%, which suggests that, in many practical applications, the estimates could be still regarded as valid ones [4], [35].

To analyze further the impact of this decorrelation factor, Fig. 17 presents the error that one would assume in the

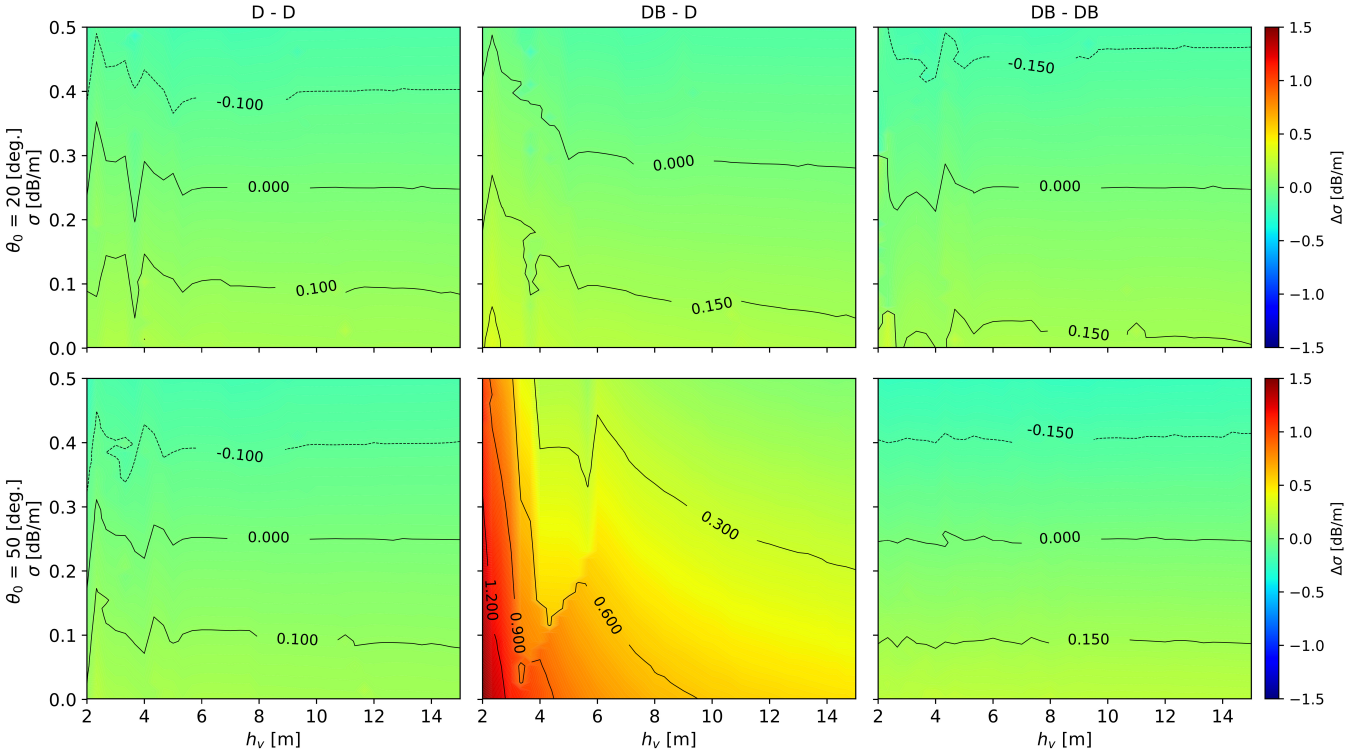

Fig. 18. Extinction error obtained using the method described in Section III-A. Model parameters: $h_v \in [2, 15]$ m, $\sigma \in [0, 0.5]$ dB/m, $\mu_{\min} = -3$ dB, and $\mu_{\max} = 3$ dB. Other system parameters: $\theta_0 = 20°$ and 50°, HoA = 30 m. (Left) Methodology D-D. (Middle) Methodology DB-D. (Right) Methodology DB-DB.

vegetation height estimates by inverting without considering the DB term for 50°, i.e., $\Delta h_{v,\text{D-DB}}$. In this case, the maximum error when the scene is wrongly characterized (case DB-D) with respect to the correct inversion (case DB-DB) is around 80 cm (i.e., 10%) at $h_v = 8.3$ m and $\sigma = 0.32$ dB/m.

3) Extinction Coefficient: The effect of the DB decorrelation over the extinction coefficient for a vertical wavenumber $\kappa_Z = 0.2$ rad/m and an HoA = 30 m is illustrated in Fig. 18, for which simulations are carried out under the same conditions of the preceding analysis (see Section IV-B2).

The error in the extinction estimates shows the same behavior for all three methodologies D-D, DB-D, and DB-DB at steep incidences. Similar to the crop scenario, the case DB-D for 50° shows a higher overestimation for h_v values below 5 m that was not evident for 20°. Again, this is a limitation due to the baseline: there is a minimum vegetation height required to have enough interferometric sensitivity to the vertical distribution of scatterers within the scene. The minimum value of vegetation height needed is scaled to the type of scene evaluated (i.e., around 30 cm for the crop scenes and around 4 m for the forests scenes), since it also depends on the HoA (i.e., 3 and 30 m for crops and forests, respectively).

The influence of the initial guess on the retrieved values follows the same general behavior commented for crops, i.e., the output estimates fluctuate around the initial value, regardless of its magnitude. As in the agriculture case, this insensitive estimation of extinction affects the reliability of the rest of the model parameters: vegetation height and ground-to-volume ratios. On average, employing a low value of extinction as input to the inversion (e.g., 0 dB/m) worsens the accuracy of the estimates, whereas a high extinction (e.g., 0.5 dB/m) improves it.

4) Ground-to-Volume Ratios: The error in the minimum and maximum ground-to-volume ratios is shown in Figs. 19 and 20, respectively. The simulated vegetation height adapted to forest scenes is $h_v = 10$ m (with $\kappa_Z = 0.2$ rad/m and an HoA = 30 m). Similarly, the extinction is fixed to an average value $\sigma = 0.25$ dB/m, characteristic of a forest scene [7]. The rest of the parameters are equal to those employed in Section IV-A4.

Results are in line with the general trend: the DB decorrelation contribution γ_{DB} is less significant for steep incidences (20°) and is only visible for oblique incidence angles (50°). Under analogous conditions, the resulting error in the $\mu_{\min}$ and $\mu_{\max}$ estimates shows the same behavior observed in the crop scenario (see Figs. 12 and 13).

Focusing on the results for 50°, the maximum error $\Delta\mu_{\min}$ is found at the ground-to-volume ratio pairs above $\mu_{\min} = 8.5$ dB and $\mu_{\max} = 9$ dB/m. This deviation in methodology DB-D is completely compensated in the DB-DB case. On the other hand, the greatest error in the estimates of the maximum ground-to-volume ratio is also found at high values of ground-to-volume ratio pairs, at $\mu_{\min} = 9.5$ dB and $\mu_{\max} = 10$ dB, following methodology DB-D.

A scene characterized by two high ground-to-volume ratios implies a dominant backscattering from the ground relative

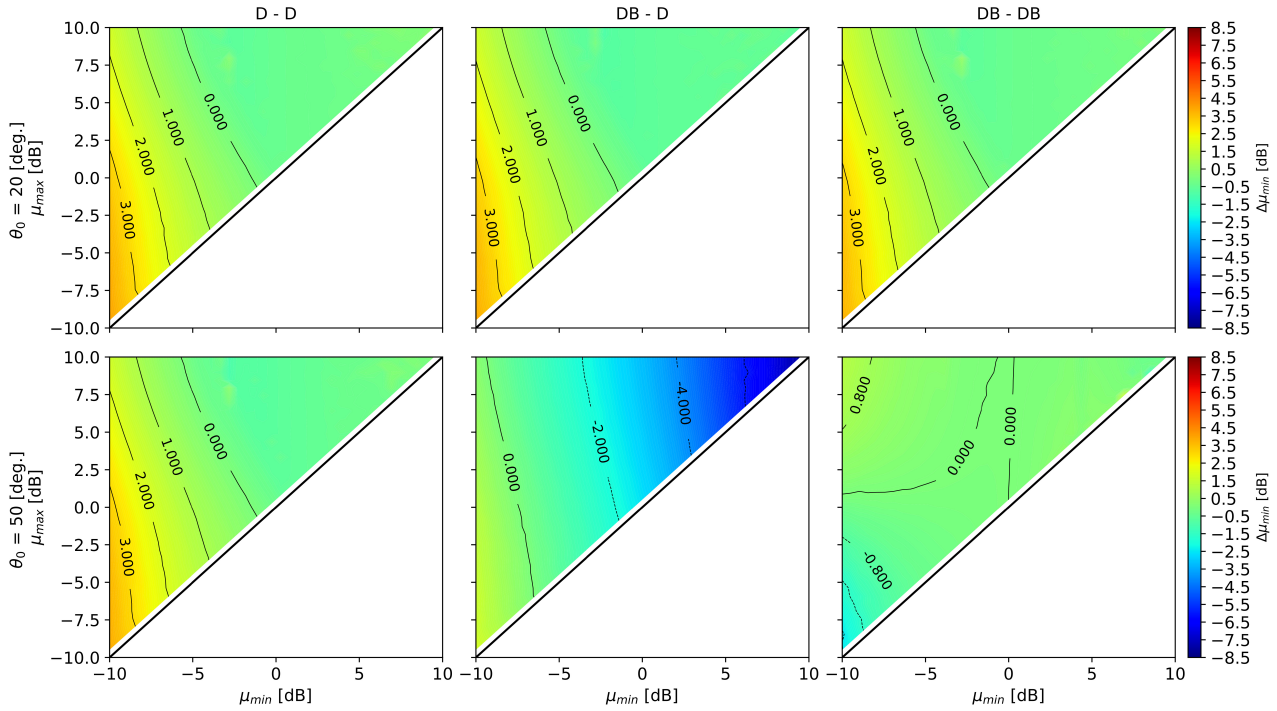

Fig. 19. Error in the minimum ground-to-volume ratio estimated using the method described in Section III-A. Model parameters: $h_v = 10$ m, $\sigma = 0.25$ dB/m, $\mu_{\min} \in [-10, 10]$ dB, and $\mu_{\max} \in= [-10, 10]$ dB. Other system parameters: $\theta_0 = 20°$ and $50°$, and HoA $= 30$ m. (Left) Methodology D-D. (Middle) Methodology DB-D. (Right) Methodology DB-DB.

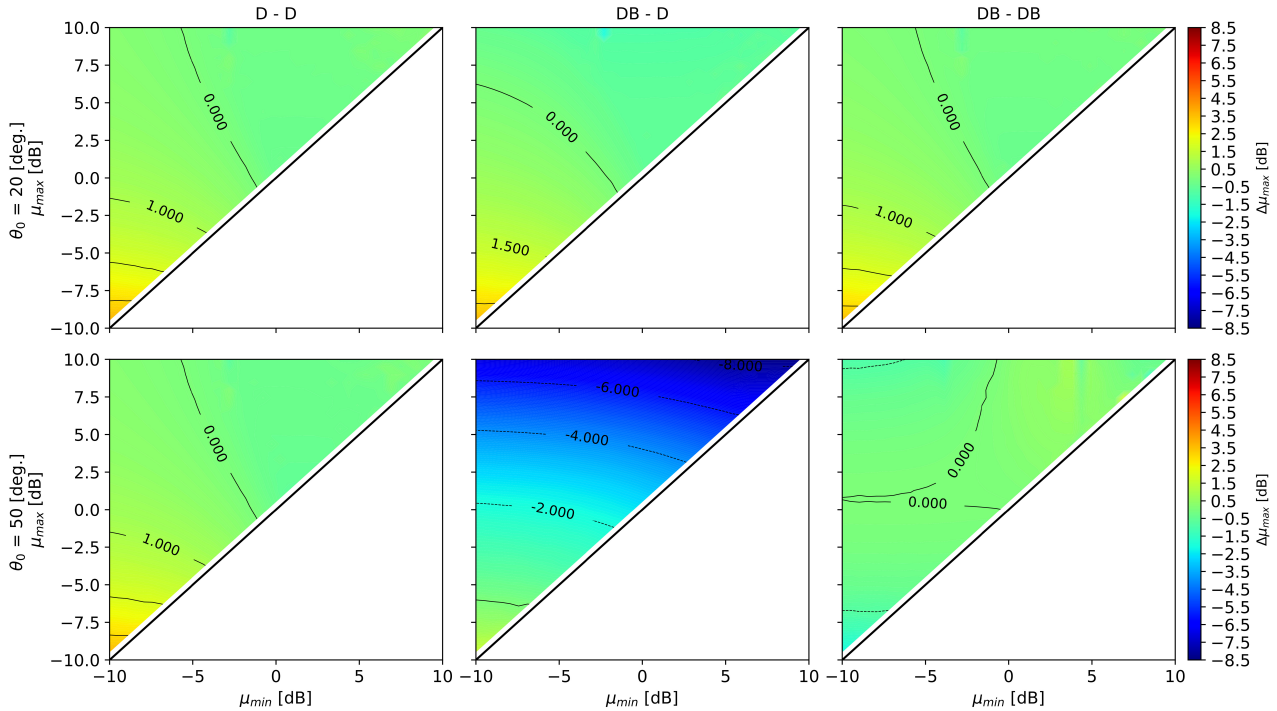

Fig. 20. Error in the maximum ground-to-volume ratio estimated using the method described in Section III-A. Model parameters: $h_v = 10$ m, $\sigma = 0.25$ dB/m, $\mu_{\min} \in [-10, 10]$ dB, and $\mu_{\max} \in= [-10, 10]$ dB. Other system parameters: $\theta_0 = 20°$ and $50°$, and HoA $= 30$ m. (Left) Methodology D-D. (Middle) Methodology DB-D. (Right) Methodology DB-DB.

to the backscattering from the volume. With a negligible volume backscatter, the coherences of the RVoG model are not along a straight line on the complex plane but concentrated at a single point, which is also very close to the radius of the circumference. This is an extreme scenario, in which the variability of the possible solutions is such that the numerical

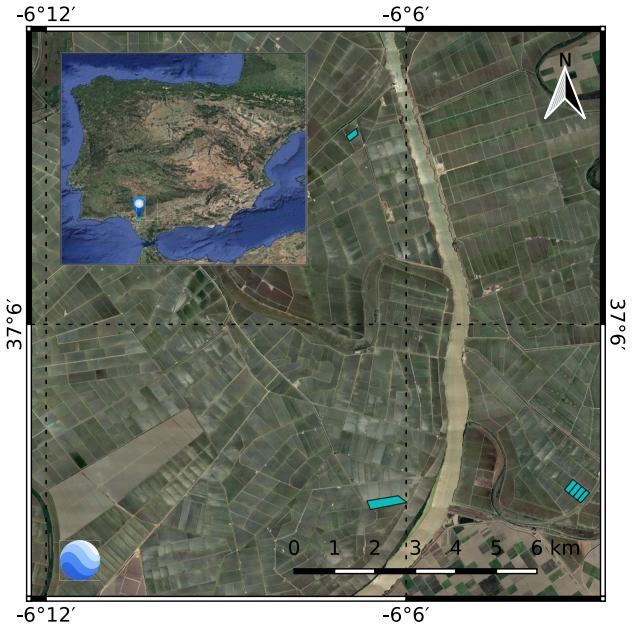

Fig. 21. Location of the Seville study area. The three test fields monitored are highlighted.

minimization may fall in local minima, thus yielding the mentioned error.

V. Analysis With Real Data

A. Test Site and Data Set

A paddy rice area is considered to analyze the effect of the DB decorrelation term on the final height estimates in a real scenario. This type of crop has been chosen, because the DB is known to dominate the ground response. The area of study is located in the mouth of the Guadalquivir river (37.1 N, 6.15 W), which covers an area of 30 km × 30 km in Seville, Southwest of Spain (see Fig. 21).

In this test site, the sowing method consists of spreading seeds randomly from an airplane over the fields, which are always flooded during the entire cultivation period, from May to October (around 135–150 days). It is important to acknowledge that this permanent flooded condition implies that the ground is going to be considered as a water surface from the radar point of view. Hence, the direct response from the ground can be neglected when compared with the DB ground response [22].

Detailed agricultural descriptors of the rice fields covering the whole growth season were collected by local farmers on a weekly basis. In particular, three parcels from the 2015 campaign have been selected for the analysis, which include phenological information according to the Biologische Bundesanstalt, Bundessortenamt und CHemische Industrie (BBCH) scale, as well as the above-water vegetation height.

In the last years, several studies have employed this test site to monitor rice growth with SAR images, such as [15] and [36]–[41], among others.

The SAR data exploited in this article were acquired during the science phase of the TanDEM-X mission, from April to September 2015. PolInSAR time-series data correspond to the HH-VV dual-pol images, obtained with three different incidence angles, namely, 23°, 30°, and 40°. The main information of these images is presented in Table IV.

TABLE IV
TanDEM-X System Parameters Over Seville

Incidence angle	HoA [m]	κ_Z [rad/m]	Date range
23 degrees	2.53	2.48	20150604–0820
30 degrees	3.49	1.80	20150526–0902
40 degrees	5.81	1.08	20150530–0906

For the steepest incidence angle of 23°, there are eight image pairs, and only six for the incidence angles of 30° and 40°. The correlation of height of ambiguity and angle of incidence must be noted [34]. Acquisitions obtained with the steepest incidence angle present the largest spatial baseline, i.e., 2.84 rad/m (and the shortest height of ambiguity, HoA = 2.53 m). In contrast, the spatial baselines of 1.8 rad/m (HoA = 3.49 m) and 1.08 rad/m (HoA = 5.81 m) are found for the incidence angles of 30° and 40°, respectively.

For the analysis, the SAR data processing detailed in [15] is carried out over the standard Coregistered Single-Look Slant-range Complex (CoSSC) product of each acquisition. In the end, the PolInSAR inversion algorithm described in Section III was applied to each pixel inside the eroded region of interest (ROI) of each parcel. The statistics of the resulting estimates (average values and standard deviations) are calculated and examined in Section V-B.

B. Experimental Results

In the analysis based on the simulations described in Section IV, the data used as input to the retrieval algorithm were obtained directly from the RVoG model, so we were assuming that the scenes were perfectly characterized by such a model. However, when it comes to real data, there is no guarantee on the matching between the scene (and hence the measured radar data) and the physical model used to describe it (i.e., RVoG). As a result, the retrieval of the RVoG parameters is also affected by this unavoidable source of uncertainty, which may have implications also on the numerical aspects of inversion. For instance, the convergence criterion (i.e., 5% of the visible RVoG line) is not fulfilled in many cases. When this happens, the optimized solutions cannot be considered as valid estimates, because the model is not properly adjusted to the data. In addition, the mismatch between the data and the model may affects the differences observed between the solutions provided by considering or not the DB term, since potentially different regions of the solution space may be accessed during the iterative optimization. These aspects must be always kept in mind when analyzing the estimates derived from real data.

In order to follow the same retrieval approach followed in the simulations, the set of initial guesses employed in the real data experiments is the same, i.e., $h_v = 1$ m, $\sigma = 5$ dB/m, $\mu_{\min} = -3$ dB, and $\mu_{\max} = 3$ dB. The effect of the initial guess will be discussed later on.

The temporal evolution of the height estimates at the Seville test site is presented in Fig. 22. Columns 1–3 correspond

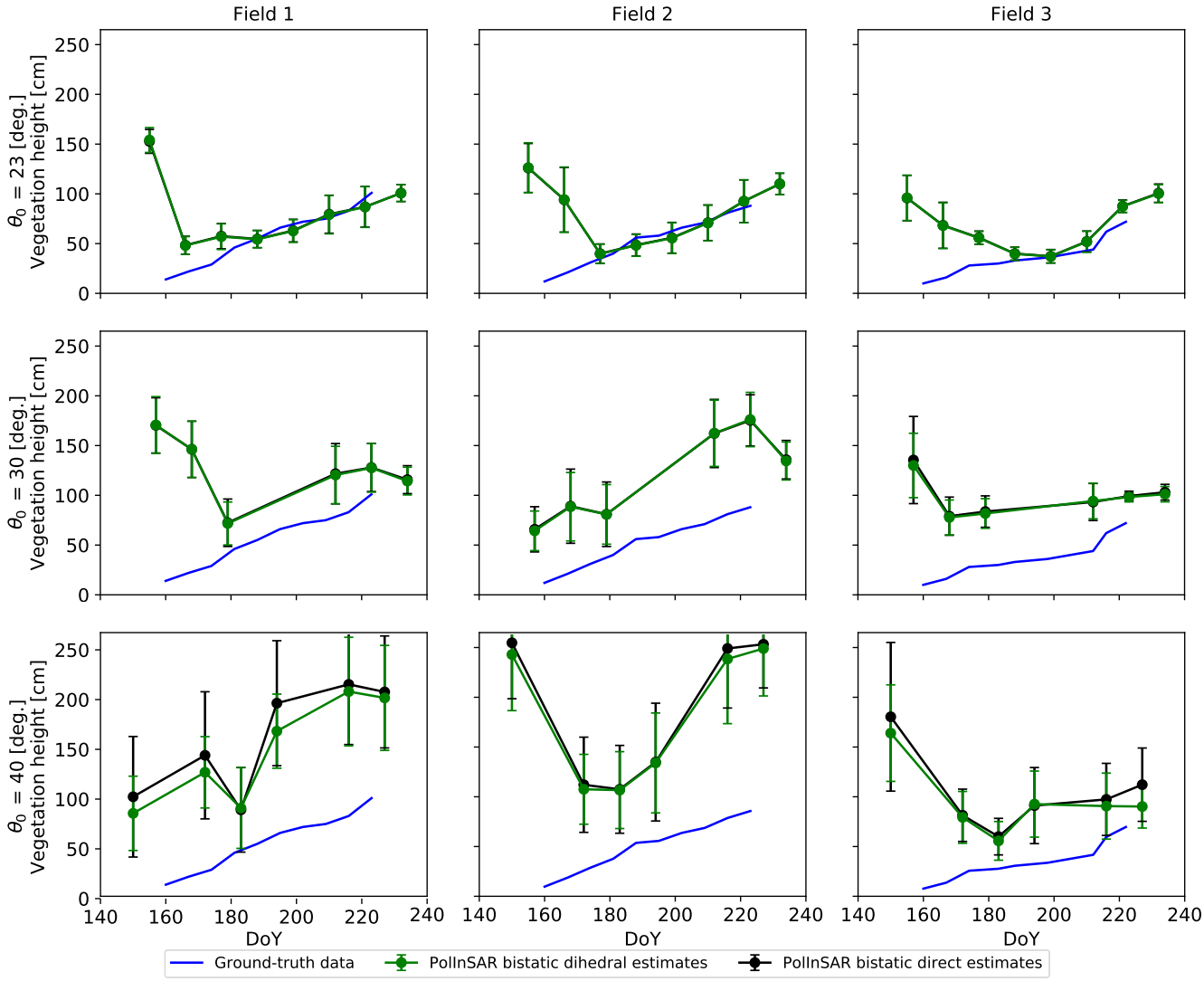

Fig. 22. Temporal evolution of the ground data (blue), and the vegetation height estimates following an inversion with the DB term (DB, green) and without it (D, black). Circles denote the average value and the error bars denote ±1 standard deviation, both computed from all pixels inside a field.

to three different fields, whereas the first, second, and third rows present the results for the incidence angles evaluated (see Table IV).

Before comparing the estimates provided by considering or not the DB, it must be reminded that when the product of vegetation height and vertical wavenumber is very small, there is not sufficient interferometric sensitivity to the vertical distribution of scatterers in the scene, which usually translates into an overestimation of vegetation height. This happens at 30° and 40° at all dates because of the associated vertical wavenumbers (see Table IV) and also at 23° at the initial dates, because the height of the plants is less than 30 cm [15].

The results shown in Fig. 22 are consistent with the simulation analysis for vegetation height retrieval in the crop scenario (see Section IV-A2). For steep incidence angles, 23° and 30°, the difference between the estimates obtained when the DB decorrelation term is considered in the inversion (method DB in Fig. 3, green plots) and when it is ignored (method D in Fig. 3, black plots) is insignificant, less than 1 cm at all dates. This difference is much more pronounced, up to 17 cm, at the shallowest incidence angle, 40°. The three fields evaluated confirm this behavior throughout the entire cultivation period.

Focusing now on the most suitable results, obtained at 23° thanks to its associated large baseline, one may observe that the overall consistency of the RVoG inversion performance is satisfied for both methodologies (DB and D), as the results in Fig. 7 already anticipated. At the acquisitions available after DoY 170, i.e., when plants are taller than 30 cm, depending on the field and the date, there appear some minor fluctuations in the height estimates with respect to the true value, but none of them is really significant. Therefore, for the X-band data acquired over paddy rice with θ_0 =23° and HoA = 2.53 m (κ_Z = 2.48 rad/m), we can conclude that there is no significant influence of the DB term on the vegetation height estimates.

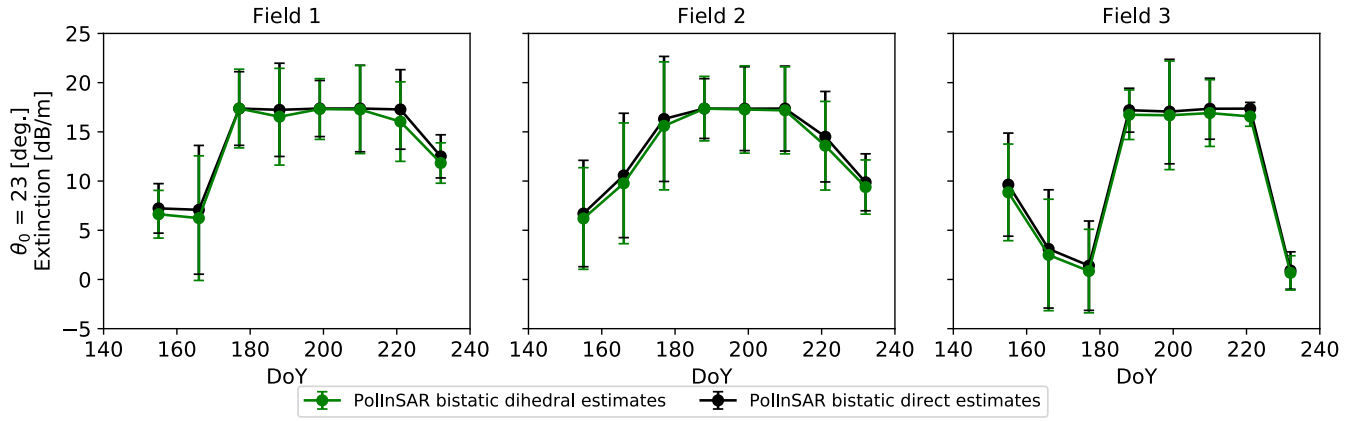

Fig. 23. Temporal evolution of the extinction estimates obtained following an inversion with the DB term (DB, green) and without it (D, black). Circles denote the average value, and error bars denote ±1 standard deviation, both computed from all pixels inside a field.

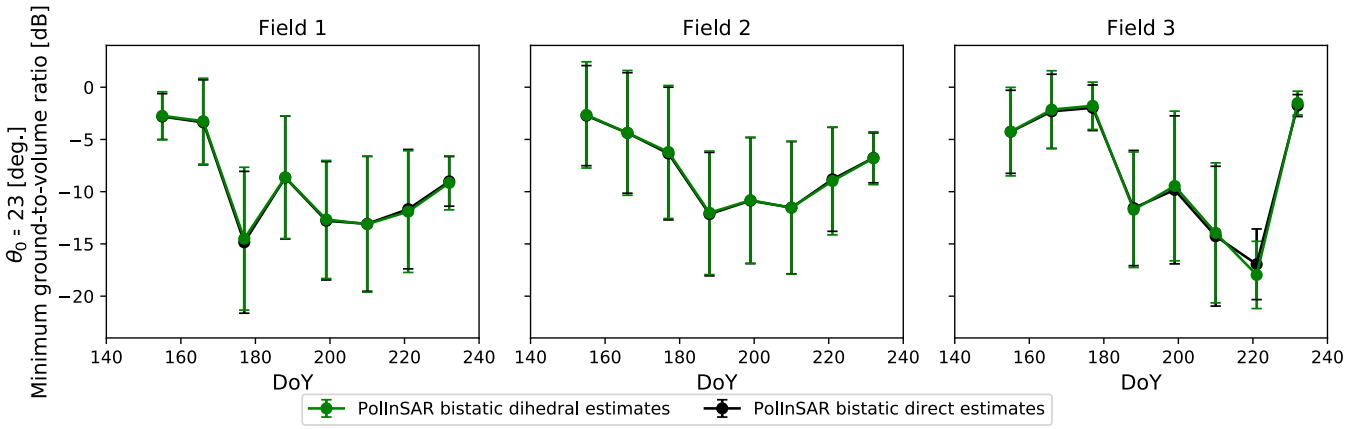

Fig. 24. Temporal evolution of the minimum ground-to-volume ratio estimates obtained following an inversion with the DB term (DB, green) and without it (D, black). Circles denote the average value and error bars denote ±1 standard deviation, both computed from all pixels inside a field.

Figs. 23–25 show the temporal evolution of the estimates of the rest of parameters obtained at 23° incidence angle, i.e., extinction, and minimum and maximum ground-to-volume ratios, respectively. Unfortunately, the ground-truth data of these parameters are not available. The reader is referred to [11], [13], [32], and [42] for the experimental measurements and estimations of the RVoG and OVoG parameters at the L-, C-, and X-bands.

Regarding the extinction estimates shown in Fig. 23 and ignoring the first two dates due to the mentioned lack of interferometric sensitivity, the values provided are around 15 dB/m in the central dates and decrease at the end of the campaign. This late decrease can be associated with the drier condition of the plant elements at late phenological stages. As suggested in [32], attenuation at the X-band is associated with the leaves (i.e., at the middle of the growing season), whereas the stalks exert a small influence in comparison (i.e., at the end of the season). However, as the standard deviation shows, there is a high variability in the estimates, which corroborates what the simulations anticipated (see Figs. 9–11 and 18): the RVoG model is less sensitive to extinction than to the vegetation height. These findings are in agreement with the inversion results in [11] and [42], in which the extinction estimates were characterized by a high variability. Once again, results following methods *D* and DB show no significant differences between them at a steep incidence angle of 23°. In summary, ignoring the DB term does not affect the estimation of the extinction at steep incidences in the case of dealing with real data.

The temporal evolution of the minimum and maximum ground-to-volume ratios is plotted in Figs. 24 and 25, respectively. At first glance, the estimates obtained following methods *D* and DB are not different from each other, as expected for a steep incidence angle (23°). The variability of the results is quite high, being higher for the minimum than for the maximum ground-to-volume ratio. Moreover, the condition $\mu_{\max} > \mu_{\min}$ is satisfied in all dates evaluated, and there is a visible correspondence between the trends followed by $\mu_{\min}$ and $\mu_{\max}$ at each one of the fields and along time. In the beginning of the cultivation period, as the plants start to grow, the estimated ground-to-volume ratios tend to decrease with increasing biomass. As previously observed in [11], [13], and [42], at high frequencies (e.g., X-band), the scattering response from the ground is weak compared

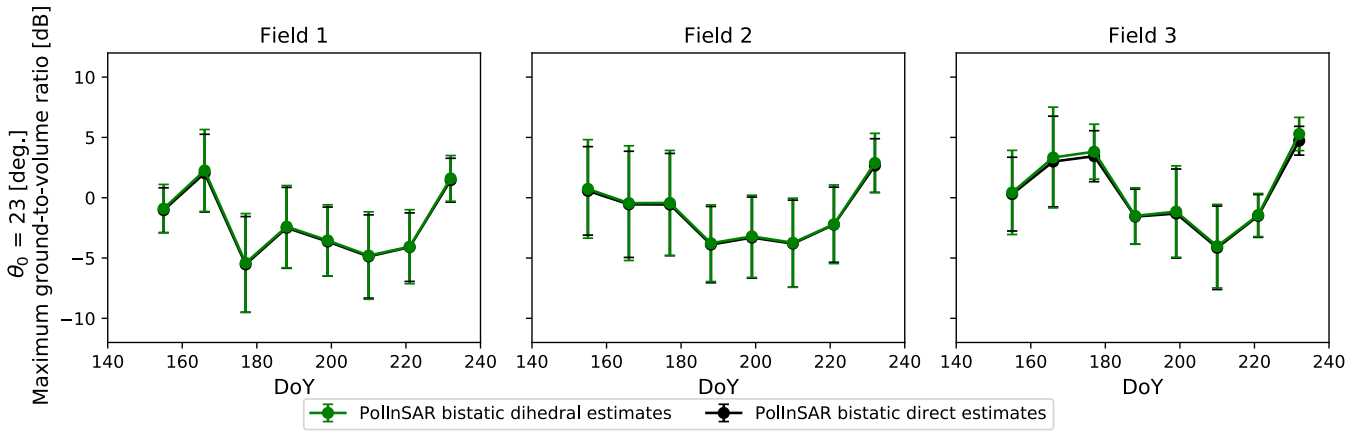

Fig. 25. Temporal evolution of the maximum ground-to-volume ratio estimates obtained following an inversion with the DB term (DB, green) and without it (D, black). Circles denote the average value and error bars denote ± 1 standard deviation, both computed from all pixels inside a field.

with the strong response from the aboveground vegetation volume due to the low penetration of the incident wave. On the other hand, both ground-to-volume ratios increase at the end of the cultivation period as a result of the drier condition of the plants. The backscatter from the volume is reduced with respect to that of the ground, which is kept flooded all along the campaign. In conclusion, the estimation of these two parameters, as it happens with vegetation height and extinction, is not affected by the inversion model selected (D or DB) with these real data acquired at a steep incidence.

VI. Conclusion

The research presented here constitutes the first complete analysis and interpretation of the DB effect on the inversion of all RVoG model parameters, including vegetation height, extinction, and ground-to-volume ratios. The influence of the DB factor present in bistatic configurations has been tested as a function of both scene and system parameters. Theoretical and numerical aspects of the inversion have been reformulated accounting for this term. In addition, the study has been conducted over the crop and forest scenes, for which the same general approach has been assessed. The algorithm has been also applied to a set of single-pass bistatic TanDEM-X data over a rice area in Spain.

The main findings from the simulations are summarized in the following list.

1) *Topography:* The influence of γ_{DB} on the z_0 estimates in both crop and forest scenarios becomes important for θ_0 above 30° and especially for low extinctions (below 5 dB/m).
2) *Vegetation Height:* The inversion approach should consider the DB for θ_0 greater than 30°. Results show that the accuracy required for the crop scenarios is higher than that for the forest scenes (with larger vegetation heights and smaller spatial baselines). In the worst case, at $\theta_0 = 50°$, the deviation caused by this decorrelation term is greater than 10% for lower vegetation heights and larger extinctions.
3) *Extinction:* The effect of ignoring the DB for short crops ($h_v < 30$ cm) is present at all incidence angles, even at the steepest ones (20°), and thus, it should always be considered. However, it has also been found that the final estimates of extinction are greatly affected by the initial guess of this unknown: the output estimates fluctuate around the initial guess, regardless of its magnitude. Therefore, in general, the resulting extinctions could not be considered as valid estimates, since the extinction is acting as a sort of fitting parameter. In the simulations, varying the initial guess of extinction affects the estimation of the rest of model parameters, i.e., vegetation height and ground-to-volume ratios.
4) *Ground-to-Volume Ratios:* Neglecting the DB term in the inversion at shallow incidences (θ_0 greater than 30°) results also in a significant underestimation in the final estimates of the minimum and maximum ground-to-volume ratios.

These conclusions derived from simulations were partially confirmed with an experimental data set acquired over rice fields at incidence angles equal to 23°, 30°, and 40°. However, the associated baselines were too short at 30° and 40° to provide enough interferometric sensitivity, hence preventing us from observing all the effects predicted in the simulations. In addition, the mismatch between the data and the RVoG model causes some differences in the behavior of the retrieval algorithm with respect to the ideal case employed in the simulations. Nonetheless, the following conclusions were drawn from the experiment with real data.

1) The retrieval of all model parameters, including vegetation height, extinction, and ground-to-volume ratios, by ignoring the DB term, i.e., regarding the ground response as dominated by direct scattering, provides virtually the same estimates as considering it at steep incidences (23°). Hence, this decorrelation term can be safely ignored in this case.
2) Regarding the central dates of the crop development, when enough interferometric sensitivity is ensured, all parameters are consistently estimated.

In summary, vegetation height, which is the most widely used output parameter in PolInSAR studies, is in general well estimated regardless of the presence of the DB decorrelation [42], provided that the incidence angle is steep enough. For oblique angles, however, this term should be considered

in the inversion. The same comments apply to the ground-to-volume ratios, despite that their final application in real cases is not as straightforward as that for vegetation height [19]. Finally, the inversion of the extinction estimates always suffers from large errors due to a general insensitivity of the PolInSAR data to this parameter [42].

ACKNOWLEDGMENT

All the TanDEM-X data were provided by the German Aerospace Center (DLR) under project NTI-POLI6736. The authors would like to thank for the support of the Federacion de Arroceros de Sevilla for providing the field data.

REFERENCES

[1] S. R. Cloude and K. P. Papathanassiou, "Polarimetric SAR interferometry," *IEEE Trans. Geosci. Remote Sens.*, vol. 36, no. 5, pp. 1551–1565, Sep. 1998.

[2] K. P. Papathanassiou and S. R. Cloude, "Single-baseline polarimetric SAR interferometry," *IEEE Trans. Geosci. Remote Sens.*, vol. 39, no. 11, pp. 2352–2363, 2001.

[3] F. Garestier, P. C. Dubois-Fernandez, and I. Champion, "Forest height inversion using high-resolution P-band pol-InSAR data," *IEEE Trans. Geosci. Remote Sens.*, vol. 46, no. 11, pp. 3544–3559, Nov. 2008.

[4] I. Hajnsek, F. Kugler, S.-K. Lee, and K. P. Papathanassiou, "Tropical-forest-parameter estimation by means of Pol-InSAR: The INDREX-II campaign," *IEEE Trans. Geosci. Remote Sens.*, vol. 47, no. 2, pp. 481–493, Feb. 2009.

[5] S.-K. Lee, F. Kugler, K. P. Papathanassiou, and I. Hajnsek, "Quantification of temporal decorrelation effects at L-band for polarimetric SAR interferometry applications," *IEEE J. Sel. Topics Appl. Earth Observ. Remote Sens.*, vol. 6, no. 3, pp. 1351–1367, Jun. 2013.

[6] F. Kugler, D. Schulze, I. Hajnsek, H. Pretzsch, and K. P. Papathanassiou, "TanDEM-X Pol-InSAR performance for forest height estimation," *IEEE Trans. Geosci. Remote Sens.*, vol. 52, no. 10, pp. 6404–6422, Oct. 2014.

[7] F. Kugler, S.-K. Lee, I. Hajnsek, and K. P. Papathanassiou, "Forest height estimation by means of Pol-InSAR data inversion: The role of the vertical wavenumber," *IEEE Trans. Geosci. Remote Sens.*, vol. 53, no. 10, pp. 5294–5311, Oct. 2015.

[8] S.-K. Lee and T. E. Fatoyinbo, "TanDEM-X Pol-InSAR inversion for mangrove canopy height estimation," *IEEE J. Sel. Topics Appl. Earth Observ. Remote Sens.*, vol. 8, no. 7, pp. 3608–3618, Jul. 2015.

[9] S. Abdullahi, F. Kugler, and H. Pretzsch, "Prediction of stem volume in complex temperate forest stands using TanDEM-X SAR data," *Remote Sens. Environ.*, vol. 174, pp. 197–211, Mar. 2016.

[10] J. M. Lopez-Sanchez, I. Hajnsek, and J. D. Ballester-Berman, "First demonstration of agriculture height retrieval with PolInSAR airborne data," *IEEE Geosci. Remote Sens. Lett.*, vol. 9, no. 2, pp. 242–246, Mar. 2012.

[11] M. Pichierri, I. Hajnsek, and K. P. Papathanassiou, "A multibaseline Pol-InSAR inversion scheme for crop parameter estimation at different frequencies," *IEEE Trans. Geosci. Remote Sens.*, vol. 54, no. 8, pp. 4952–4970, Aug. 2016.

[12] M. Pichierri and I. Hajnsek, "Comparing performances of crop height inversion schemes from multifrequency Pol-InSAR data," *IEEE J. Sel. Topics Appl. Earth Observ. Remote Sens.*, vol. 10, no. 5, pp. 1727–1741, May 2017.

[13] M. Pichierri, I. Hajnsek, S. Zwieback, and B. Rabus, "On the potential of polarimetric SAR interferometry to characterize the biomass, moisture and structure of agricultural crops at L-, C- and X-bands," *Remote Sens. Environ.*, vol. 204, pp. 596–616, Jan. 2018.

[14] E. Erten, J. M. Lopez-Sanchez, O. Yuzugullu, and I. Hajnsek, "Retrieval of agricultural crop height from space: A comparison of SAR techniques," *Remote Sens. Environ.*, vol. 187, pp. 130–144, Dec. 2016.

[15] J. M. Lopez-Sanchez, F. Vicente-Guijalba, E. Erten, M. Campos-Taberner, and F. J. Garcia-Haro, "Retrieval of vegetation height in rice fields using polarimetric SAR interferometry with TanDEM-X data," *Remote Sens. Environ.*, vol. 192, pp. 30–44, Apr. 2017.

[16] O. Yuzugullu, E. Erten, and I. Hajnsek, "Assessment of paddy rice height: Sequential inversion of coherent and incoherent models," *IEEE J. Sel. Topics Appl. Earth Observ. Remote Sens.*, vol. 11, no. 9, pp. 3001–3013, Sep. 2018.

[17] S.-K. Lee, S. Yoon, and J.-S. Won, "Vegetation height estimate in rice fields using single polarization TanDEM-X science phase data," *Remote Sens.*, vol. 10, no. 11, p. 1702, 2018.

[18] R. N. Treuhaft, S. N. Madsen, M. Moghaddam, and J. J. van Zyl, "Vegetation characteristics and underlying topography from interferometric radar," *Radio Sci.*, vol. 31, no. 6, pp. 1449–1485, Nov. 1996.

[19] R. N. Treuhaft and P. R. Siqueira, "Vertical structure of vegetated land surfaces from interferometric and polarimetric radar," *Radio Sci.*, vol. 35, no. 1, pp. 141–177, Jan. 2000.

[20] S. R. Cloude and K. P. Papathanassiou, "Three-stage inversion process for polarimetric SAR interferometry," *IEE Proc.-Radar, Sonar Navigat.*, vol. 150, no. 3, pp. 125–134, 2003.

[21] J. D. Ballester-Berman and J. M. Lopez-Sanchez, "Coherence loci for a homogeneous volume over a double-bounce ground return," *IEEE Geosci. Remote Sens. Lett.*, vol. 4, no. 2, pp. 317–321, Apr. 2007.

[22] J. D. Ballester-Berman and J. M. Lopez-Sanchez, "Combination of direct and double-bounce ground responses in the homogeneous oriented volume over ground model," *IEEE Geosci. Remote Sens. Lett.*, vol. 8, no. 1, pp. 54–58, Jan. 2011.

[23] N. Romero-Puig, J. M. Lopez-Sanchez, and J. D. Ballester-Berman, "Effect of the double-bounce contribution in PolInSAR-based height estimates of rice crops using TanDEM-X bistatic data," in *Proc. IEEE Int. Geosci. Remote Sens. Symp. (IGARSS)*, Jul. 2018, pp. 387–390.

[24] S. R. Cloude, *Polarisation: Applications in Remote Sensing*. London, U.K.: Oxford Univ. Press, 2009.

[25] T. Flynn, M. Tabb, and R. Carande, "Coherence region shape extraction for vegetation parameter estimation in polarimetric SAR interferometry," in *Proc. IEEE Int. Geosci. Remote Sens. Symp.*, vol. 5, Jun. 2002, pp. 2596–2598.

[26] E. Colin-Koeniguer, "Apport de la polarimétriea l'interférométrie radar pour l'estimation des hauteurs de cibles et de parametres de forêt," Ph.D. dissertation, Traitement du signal et de l'image, Universite Pierre et Marie Curie, Paris, France, Sep. 2005.

[27] R. N. Treuhaft and S. R. Cloude, "The structure of oriented vegetation from polarimetric interferometry," *IEEE Trans. Geosci. Remote Sens.*, vol. 37, no. 5, pp. 2620–2624, Jun. 1999.

[28] S. Oveisgharan, S. Saatchi, and S. Hensley, "Sensitivity of pol-InSAR measurements to vegetation parameters," *IEEE Trans. Geosci. Remote Sens.*, vol. 53, no. 12, pp. 6561–6572, Dec. 2015.

[29] Q. Xie, C. Wang, J. Zhu, H. Fu, and C. Wang, "Improvement of forest height retrieval by integration of dual-baseline PolInSAR data and external DEM data," *Int. Arch. Photogram., Remote Sens. Spatial Inf. Sci.*, vol. 40, pp. 185–189, Jun. 2015.

[30] Q. Xie, J. Zhu, C. Wang, H. Fu, J. M. Lopez-Sanchez, and J. D. Ballester-Berman, "A modified dual-baseline PolInSAR method for forest height estimation," *Remote Sens.*, vol. 9, no. 8, pp. 1–17, 2017.

[31] H. Chen, S. R. Cloude, D. G. Goodenough, D. A. Hill, and A. Nesdoly, "Radar forest height estimation in mountainous terrain using TanDEM-X coherence data," *IEEE J. Sel. Topics Appl. Earth Observ. Remote Sens.*, vol. 11, no. 10, pp. 3443–3452, Oct. 2018.

[32] F. T. Ulaby, A. Tavakoli, and B. A. Thomas, "Microwave propagation constant for a vegetation canopy with vertical stalks," *IEEE Trans. Geosci. Remote Sens.*, vol. GE-25, no. 6, pp. 714–725, Nov. 1987.

[33] J. M. Lopez-Sanchez and J. D. Ballester-Berman, "Potentials of polarimetric SAR interferometry for agriculture monitoring," *Radio Sci.*, vol. 44, no. 2, pp. 1–20, 2009, doi: 10.1029/2008RS004078.

[34] J. M. Lopez-Sanchez, F. Vicente-Guijalba, A. Mestre-Quereda, N. Romero, and E. Erten, "Influence of incidence angle and baseline on the retrieval of biophysical parameters of rice fields by means of polarimetric SAR interferometry with TanDEM-X data," in *Proc. IEEE Int. Geosci. Remote Sens. Symp. (IGARSS)*, Jul. 2017, pp. 926–929.

[35] H. Chen, S. R. Cloude, and D. G. Goodenough, "Forest canopy height estimation using TanDEM-X coherence data," *IEEE J. Sel. Topics Appl. Earth Observ. Remote Sens.*, vol. 9, no. 7, pp. 3177–3188, Jul. 2016.

[36] O. Yuzugullu, E. Erten, and I. Hajnsek, "Rice growth monitoring by means of X-band co-polar SAR: Feature clustering and BBCH scale," *IEEE Geosci. Remote Sens. Lett.*, vol. 12, no. 6, pp. 1218–1222, Jun. 2015.

[37] C. Kucuk, G. Taskin, and E. Erten, "Paddy-rice phenology classification based on machine-learning methods using multitemporal co-polar X-band SAR images," *IEEE J. Sel. Topics Appl. Earth Observ. Remote Sens.*, vol. 9, no. 6, pp. 2509–2519, Jun. 2016.

[38] J. M. Lopez-Sanchez, J. D. Ballester-Berman, and I. Hajnsek, "First results of rice monitoring practices in Spain by means of time series of TerraSAR-X dual-pol images," *IEEE J. Sel. Topics Appl. Earth Observ. Remote Sens.*, vol. 4, no. 2, pp. 412–422, Jun. 2011.

[39] J. M. Lopez-Sanchez, S. R. Cloude, and J. D. Ballester-Berman, "Rice phenology monitoring by means of SAR polarimetry at X-band," *IEEE Trans. Geosci. Remote Sens.*, vol. 50, no. 7, pp. 2695–2709, Jul. 2012.
[40] J. M. Lopez-Sanchez, F. Vicente-Guijalba, J. D. Ballester-Berman, and S. R. Cloude, "Polarimetric response of rice fields at C-band: Analysis and phenology retrieval," *IEEE Trans. Geosci. Remote Sens.*, vol. 52, no. 5, pp. 2977–2993, May 2014.
[41] J. M. Lopez-Sanchez, F. Vicente-Guijalba, J. D. Ballester-Berman, and S. R. Cloude, "Influence of incidence angle on the coherent copolar polarimetric response of rice at X-band," *IEEE Geosci. Remote Sens. Lett.*, vol. 12, no. 2, pp. 249–253, Feb. 2015.
[42] J. M. Lopez-Sanchez, J. D. Ballester-Berman, and Y. Marquez-Moreno, "Model limitations and parameter-estimation methods for agricultural applications of polarimetric SAR interferometry," *IEEE Trans. Geosci. Remote Sens.*, vol. 45, no. 11, pp. 3481–3493, Nov. 2007.

Noelia Romero-Puig (Student Member, IEEE) received the B.Sc. degree in sound and image in telecommunications engineering and the M.Sc. degree in telecommunication engineering from the University of Alicante, Alicante, Spain, in 2016 and 2018, respectively, where she is pursuing the Ph.D. degree with the Signals, Systems and Telecommunication Group.

Her research interest includes monitoring of agricultural crops by means of SAR interferometry (InSAR) and polarimetric SAR interferometry (PolInSAR) techniques.

Ms. Romero-Puig was a recipient of the Award for Best Final Master's Project in Remote Sensing defended in Spain in 2018 of the IEEE GRSS Spanish Chapter and the Hisdesat Award for the Best Final Master's Project in Government Satellite Services by the Official College of Telecommunications Engineers (COIT).

Juan M. Lopez-Sanchez (Senior Member, IEEE) was born in Alicante, Spain, in 1972. He received the Ingeniero (M.S.) and Doctor Ingeniero (Ph.D.) degrees in telecommunication engineering from the Technical University of Valencia (UPV), Valencia, Spain, in 1996 and 2000, respectively.

From 1998 to 1999, he worked as a Pre-Doctoral Grantholder with the Joint Research Centre, Space Applications Institute, European Commission, Ispra, Italy. Since 2000, he has been leading the Signals, Systems and Telecommunication Group, University of Alicante, Alicante, where he has been a Full Professor since November 2011. He has coauthored more than 75 articles in refereed journals and more than 120 papers and presentations in international conferences and symposia. His main research interests include microwave remote sensing for inversion of biophysical parameters, polarimetric and interferometric techniques, and applications of radar remote sensing in agriculture and geophysics.

Dr. Lopez-Sanchez received the Indra Award for the best Ph.D. thesis about radar in Spain in 2001. From 2006 to 2012, he was the Chair of the Spanish Chapter of the IEEE Geoscience and Remote Sensing Society.

J. David Ballester-Berman received the M.Sc. degree in telecommunication engineering from the Technical University of Valencia, Valencia, Spain, in 2000, and the Ph.D. degree from the University of Alicante, Alicante, Spain, in 2007.

From 2000 to 2001, he was a Support Engineer in the development of software tools for the planning and design of terrestrial digital television systems. Since 2001, he has been with the Signals, Systems and Telecommunication Group, University of Alicante, carrying out educational and research tasks. His research interests include SAR polarimetry and polarimetric SAR interferometry techniques for earth observation applications.